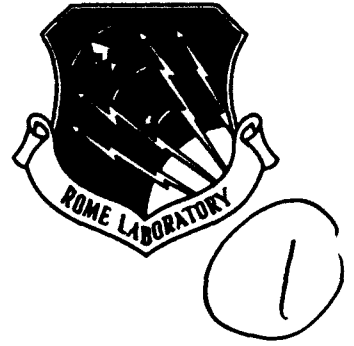


RL-TR-94-104
Final Technical Report
August 1994



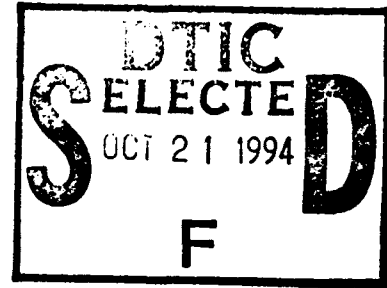
TRUE TIME DELAY BEAMFORMING

AD-A285 683



Essex Corporation

Leslie H. Gesell and Richard E. Feinleib



DTIC QUALITY INSPECTED 2

APPROVED FOR PUBLIC RELEASE; DISTRIBUTION UNLIMITED.

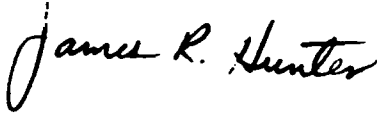
105A/ **94-32745**

Rome Laboratory
Air Force Materiel Command
Griffiss Air Force Base, New York

This report has been reviewed by the Rome Laboratory Public Affairs Office (PA) and is releasable to the National Technical Information Service (NTIS). At NTIS it will be releasable to the general public, including foreign nations.

RL-TR-94-104 has been reviewed and is approved for publication.

APPROVED:



JAMES R. HUNTER
Project Engineer

FOR THE COMMANDER:



LUKE L. LUCAS, Colonel, USAF
Deputy Director
Surveillance & Photonics Directorate

If your address has changed or if you wish to be removed from the Rome Laboratory mailing list, or if the addressee is no longer employed by your organization, please notify RL (OCPC) Griffiss AFB NY 13441. This will assist us in maintaining a current mailing list.

Do not return copies of this report unless contractual obligations or notices on a specific document require that it be returned.

REPORT DOCUMENTATION PAGE

Form Approved
OMB No. 0704-0188

Public reporting burden for this collection of information is estimated to average 1 hour per response, including the time for reviewing instructions, searching existing data sources, gathering and maintaining the data needed, and completing and reviewing the collection of information. Send comments regarding this burden estimate or any other aspect of this collection of information, including suggestions for reducing this burden, to Washington Headquarters Services, Directorate for Information Operations and Reports, 1215 Jefferson Davis Highway, Suite 1204, Arlington, VA 22202-4302, and to the Office of Management and Budget, Paperwork Reduction Project (0704-0188), Washington, DC 20503.

1. AGENCY USE ONLY (Leave Blank)		2. REPORT DATE August 1994		3. REPORT TYPE AND DATES COVERED Final Feb 92 - Feb 94	
4. TITLE AND SUBTITLE TRUE TIME DELAY BEAMFORMING				5. FUNDING NUMBERS C - F30602-92-C-0018 PE - 63726F PR - 2863 TA - 92 WU - 55	
6. AUTHOR(S) Leslie H. Gesell and Richard E. Feinleib					
7. PERFORMING ORGANIZATION NAME(S) AND ADDRESS(ES) Essex Corporation 9150 Guilford Rd. Columbia MD 21046-1891				8. PERFORMING ORGANIZATION REPORT NUMBER N/A	
9. SPONSORING/MONITORING AGENCY NAME(S) AND ADDRESS(ES) Rome Laboratory (OCPC) 25 Electronic Pky Griffiss AFB NY 13441-4515				10. SPONSORING/MONITORING AGENCY REPORT NUMBER RL-TR-94-104	
11. SUPPLEMENTARY NOTES Rome Laboratory Project Engineer: James R. Hunter/OCPC/(315) 330-3143					
12a. DISTRIBUTION/AVAILABILITY STATEMENT Approved for public release; distribution unlimited.				12b. DISTRIBUTION CODE	
13. ABSTRACT (Maximum 200 words) Wide aperture arrays for transmitting and receiving wideband signals suffer beam broadening when steered away from the array normal using phase delays between the array elements. This beam dispersion is eliminated if time delays instead of phase shifts are used between antenna array elements. This report represents the results of a project to demonstrate the proof-of-principle of an acousto-optic signal processing concept that generates and controls, with a single tone, the set of time delays required for linear antenna array beamforming. This acousto-optic concept allows an array to scan a beam rapidly over a continuum of angles. In the approach described in this report, the time delays between elements are generated by using an acousto-optic Bragg cell as a continuous delay line, and indirectly tapping selected points in the Bragg cell to the output. This optical tapping is controlled with a second Bragg cell and other standard passive optical elements. Included in this concept is a passive optical element to ensure that the phase shifts of the carrier of the time delayed signals will be correct at the RF of the array. The time-delay controller also provides the proper relative phases between the carriers of the time delayed signals at the RF of the antenna array. A proof-of-principle breadboard of the time delay controller was assembled. Results of the demonstration of the breadboard are described.					
14. SUBJECT TERMS Optical Time Delay, Optical Beamforming, Acousto-optics, Beam Steering				15. NUMBER OF PAGES 110	
				16. PRICE CODE	
17. SECURITY CLASSIFICATION OF REPORT UNCLASSIFIED		18. SECURITY CLASSIFICATION OF THIS PAGE UNCLASSIFIED		19. SECURITY CLASSIFICATION OF ABSTRACT UNCLASSIFIED	
				20. LIMITATION OF ABSTRACT UL	

TABLE OF CONTENTS

	PAGE
ABSTRACT	1
1. INTRODUCTION	2
1.1 Identification and Significance of the Problem.....	2
1.2 Project Objectives.....	3
2. DESCRIPTION OF TIME DELAY CONTROLLERS FOR BEAM STEERING	5
2.1 Architecture for Linear Transmitting Arrays.....	5
2.2 Architecture for Linear Receiving Arrays.....	8
3. STEERING PLANAR ARRAYS	9
4. TECHNICAL CONSIDERATIONS.....	11
4.1 Removal of Steering Signal Doppler Shift.....	11
4.2 Relationship Between Phases	11
4.2.1 Providing Correct Phases at RF	11
4.2.2 Providing Phases with Small Uncertainties	13
5. PROOF-OF-PRINCIPLE DEMONSTRATION	13
6. REALIZABILITY FOR REAL APPLICATIONS	17
7. CONCLUSIONS.....	18
8. REFERENCES.....	18
9. APPENDIX A	

LIST OF FIGURES

	PAGE
Figure 1. Work Plan.....	4
Figure 2. Architecture for linear transmitting arrays.....	5
Figure 3. Tapping the signal Bragg cell on the photodiode.....	6
Figure 4. Architecture for a receiving array.....	8
Figure 5. Planar array.....	9
Figure 6. Cascading of time delay controllers to steer a planar array.....	10
Figure 7. Removal of steering signal Doppler.....	11
Figure 8. Use of wedge to provide time delay dependent phase adjustment.....	12
Figure 9. Proof-of-principle breadboard.....	14
Figure 10. Phase difference versus signal frequency for a steering frequency of 49.5 MHz.....	15
Figure 11. Time delay versus frequency of the steering signal.....	16

ABSTRACT

Wide aperture arrays for transmitting and receiving wideband signals suffer beam broadening when steered away from the array normal using phase delays between the array elements. This beam dispersion is eliminated if time delays instead of phase shifts are used between antenna array elements. This report presents the results of a project to demonstrate the proof-of-principle of an acousto-optic signal processing concept that generates and controls, with a single tone, the set of time delays required for linear antenna array beamforming. This acousto-optic concept allows an array to scan a beam rapidly over a continuum of angles.

In the approach described in this report, the time delays between elements are generated by using an acousto-optic Bragg cell as a continuous delay line, and indirectly tapping selected points in the Bragg cell to the output. This optical tapping is controlled with a second Bragg cell and other standard passive optical elements. Included in this concept is a passive optical element to ensure that the phase shifts of the carrier of the time delayed signals will be correct at the RF of the array.

The time-delay controller also provides the proper relative phases between the carriers of the time delayed signals at the RF of the antenna array. A proof-of-principle breadboard of the time delay controller was assembled. The demonstration of the proof-of-principle breadboard shows that the time delays of a signal can be precisely controlled with a single steering tone, and that the relationship between time delays (pointing direction of the RF array) and the frequency of the steering tone is linear.

Accession For	
NTIS CRA&I	<input checked="" type="checkbox"/>
DTIC TAB	<input type="checkbox"/>
Unannounced	<input type="checkbox"/>
Justification	
By	
Distribution /	
Availability Codes	
Dist	Avail and/or Special
A-1	

1. INTRODUCTION

1.1 Identification and Significance of the Problem

Wide aperture, wide bandwidth phase steered array antennas suffer beam broadening when steered away from the array normal. Using time delays rather than phase delays between the array elements eliminates this beam dispersion. A brute force approach for implementing true time delay beamforming is to switch in different lengths of signal transmission delay lines between the common signal source and the antenna array elements; however, this approach can be bulky and cumbersome for scanning an array with a large number of elements over a wide range of nearly continuous angles.

A number of investigators¹⁻¹¹ have proposed using optical signal processing technologies for both phase and time delay beamforming. This report describes a Rome Laboratory funded project conducted by Essex to demonstrate the proof-of-principle of an acousto-optic controller invented by Essex¹²⁻¹⁴ to generate and rapidly change the set of time delays of a signal for true time delay steering. The Essex approach is to use an acousto-optic Bragg cell as a delay line and to use a second steering Bragg cell to control the points in the signal delay line Bragg cell that are tapped to the output. This approach allows a beam to be rapidly scanned over a continuum of angles by changing the frequency of a single tone that drives the steering Bragg cell in this architecture. The architecture of the time delay controller is simple and does not lead to a bulky and complex implementation: the required hardware can fit into a small, light-weight, rugged package and consumes a small amount of power.

In addition to properly controlling the time delays of the modulation envelope of the signal, the time-delay controller also provides the proper relative phases between the carriers of the time delayed signals at the RF of the antenna array.

The following is a summary of the potential capabilities of the Essex approach for true time delay beam steering transmitting and receiving arrays:

- For linear arrays, the delays for all of the array elements or subarrays are obtained in one compact module.
- Time delays can be finely controlled to approximately ± 10 picoseconds or less.
- A continuum of delays are achievable covering a wide range of values. ± 250 nanoseconds of delay for a 1 GHz bandwidth signal can be obtained at the fine resolution.

- Control of RF array beam pointing direction is simple. Changing the frequency of one steering signal (a tone) changes all the time delays and the pointing direction of the RF array beam.
- The proper relationship between the time delays is maintained for a beam in any desired direction.
- The amplitude dependence of the time delayed signal on time delay is negligible.
- The relative phases of the carriers of the time delayed signals are correct when up-converted to the RF of the array for pointing the array in the desired direction.
- For two-dimensional arrays, an elevation time delay module is cascaded with azimuth time delay modules to provide the time delays for the sub-arrays. For example, eleven time delay modules will control a two-dimensional array with 10x10 sub-arrays.

A proof-of-principle breadboard version of the time delay controller was assembled. The primary objective of this breadboard was to demonstrate the ability to finely control time delays, and to show that time delays are proportional to the frequency of the steering signal. To maintain a narrow beam as an array is steered with time delays, it is necessary that the relationship between the relative time delays between a reference element and the other elements of the array be proportional to one another. The fact that the time delays vary linearly with the frequency of the steering signal, and the ability to design into the time delay controller the proportionality constants between steering signal frequency and time delays, means that, given the parameters of an array, the Essex time delay controller can be designed to steer the array over a wide field of view with a single simple steering signal.

Results of the demonstration of the breadboard, presented in this report, show that the difference in time delays between two signals varies linearly with frequency of the steering signal.

1.2 Project Objectives

The objectives of this project were to investigate and validate the feasibility, and to determine the advantages and limits, of using acousto-optic signal processing concepts for true time delay beamforming and steering. These objectives were accomplished through analysis (Task 1) and laboratory demonstration (Task 2). The work plan for accomplishing these objectives is shown in Figure 1.

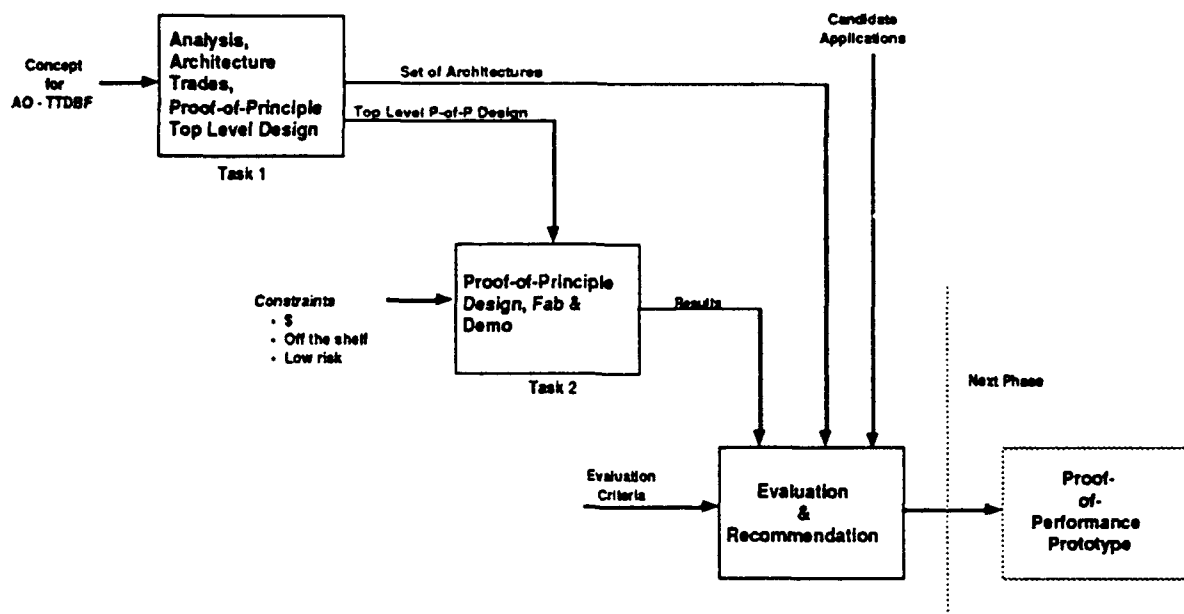


Figure 1. Work Plan

Analysis was performed on Task 1 to gain an understanding of how each of the architectures originally considered generates and controls the time delays, to establish the parametric relationships between the beamforming performance parameters and the architecture design and implementing hardware parameters, and to perform a top level design of a feasibility unit to be demonstrated in Task 2. The results of Task 1 are documented in the Annual Status Report, dated March 11, 1993. (Appendix A)

On Task 2 a proof-of-principle breadboard version of the true time delay controller was designed, assembled and demonstrated in the Essex laboratory. This breadboard is described in Section 5 of this report. This breadboard generated two delays of an 80 MHz bandwidth signal. Analysis of laboratory measurements, described in Section 5, demonstrates the ability to finely control time delays with a steering tone, and demonstrates the linearity between the steering frequency and time delays.

2. DESCRIPTION OF TIME DELAY CONTROLLERS FOR BEAM STEERING

The time delays of a wideband signal are generated in the Essex time-delay controller by using a wideband bulk acousto-optic Bragg cell as a delay line. A second Bragg cell is used to dynamically control which points in the signal Bragg cell are indirectly tapped to the output.

2.1 Architecture for Linear Transmitting Arrays

The acousto-optic architecture shown in Figure 2 generates and controls a set of time delays for linear transmitting arrays. The time delayed signals are obtained from the detector array, an array of wideband photodiodes. The time delayed signal out of each photodiode is routed to a corresponding element or sub-array of the RF array.

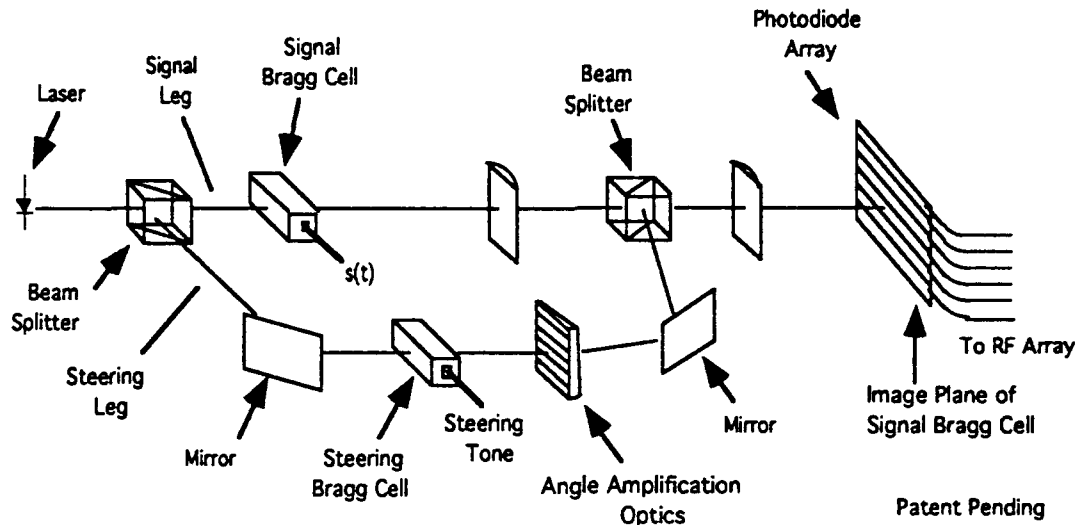


Figure 2. Architecture for linear transmitting arrays

The signal $s(t)$ to be transmitted by the linear array drives the acousto-optic signal Bragg cell in the signal leg of the interferometer. Coherent light from the laser passing through this Bragg cell is modulated by delayed replicas of signal $s(t)$. The signal Bragg cell is imaged across each photodiode of a column array of wideband photodiodes. The result is that a time-delayed replica of the signal $s(t)$ illuminates each of the photodiodes. Time delay is proportional to horizontal distance along each photodiode.

The optical beam traveling through the steering leg of the interferometer is focused to a spot on each of the photodiodes. As shown in Figure 3 and the following mathematical description, heterodyne detection on a photodiode of the steering beam spot with the signal imaged from the signal Bragg cell in effect taps the signal Bragg cell. The output signal from the photodiode is a time delayed version of the signal driving the signal Bragg cell with the delay determined by the horizontal location of the steering beam spot on the photodiode.

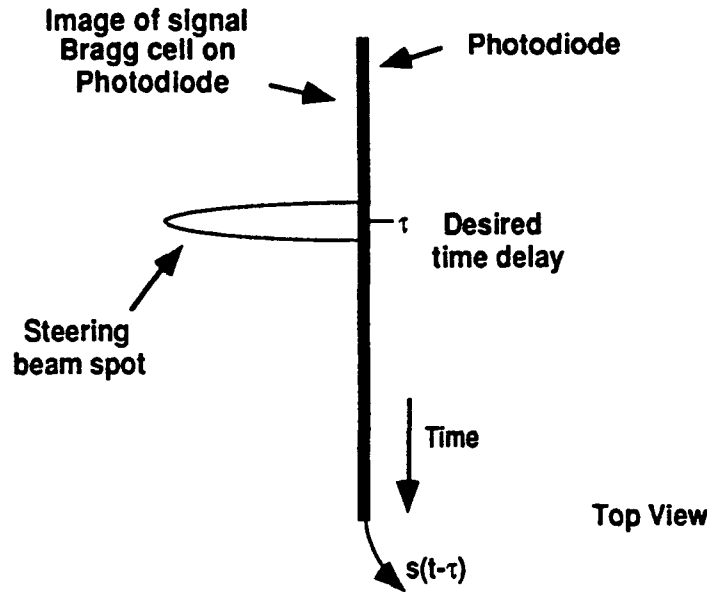


Figure 3. Tapping the signal Bragg cell on the photodiode

The wideband signal on a photodiode as a function of horizontal position τ' (time delay) is

$$s(t - \tau')e^{j2\pi f_0 t}, \quad (1)$$

where f_0 is the optical carrier frequency and t is time. The steering beam signal on the photodiode is

$$r(\tau')e^{j2\pi(f_0 + f_{\text{steer}})t}. \quad (2)$$

where f_{steer} is the frequency of the steering signal.

The output, $d(t)$, of the photodiode is the square-law detection at each instant of time of the sum of the wideband signal and the steering beam, spatially integrated along the length of the photodiode:

$$d(t) = \int_{t_a}^0 \left| r(\tau') e^{j2\pi(f_0 + f_{\text{steer}})t} + s(t - \tau') e^{j2\pi f_0 t} \right|^2 d\tau', \quad (3)$$

$$= \text{bias} + 2 \operatorname{Re} \left[\int_{t_a}^0 s(t - \tau') \cdot r^*(\tau') e^{-j2\pi f_{\text{steer}} t} d\tau' \right], \quad (4)$$

where $\operatorname{Re}[\]$ denotes the real part of the complex quantity in the brackets.

The amplitude shape of the steering beam spot is given by the function $W(\tau')$ and is centered on the detector at position τ :

$$r(\tau') = W(\tau' - \tau). \quad (5)$$

Ideally, the width of the steering beam spot is infinitesimally small, i.e.,

$$W(\tau' - \tau) = \delta(\tau' - \tau), \quad (6)$$

so that the output of the photodiode is a time delayed, frequency shifted, replica of the input signal driving the wideband signal Bragg cell:

$$d(t) = \text{bias} + 2 \operatorname{Re} \left[s(t - \tau) e^{-j2\pi f_{\text{steer}} t} \right]. \quad (7)$$

As indicated below, the Doppler shift represented by the exponential in Equation (7) can be trivially removed when upshifting from the IF of the time-delay controller to the RF of the array.

In actual implementations, W has finite width as determined by the optics in the time-delay controller. The upper frequency content of the output signal is limited to the inverse of the width of W . The optical design parameters are chosen so that the width of the spot on the photodiode is small enough to prevent low pass filtering spectral components of interest in the wideband signal.

In order to form a beam making an angle α to the array normal, the time delay difference τ required between the signals fed to two elements of an RF array, with separation b between the two elements, is given by

$$\tau = \frac{b \sin(\alpha)}{c}, \quad (8)$$

where c is the speed of light. So, when scanning a planar RF array, the difference in the time delays of the signals to any two elements of the array must be proportional to the separation between the array elements for all scan angles within the field of view of the antenna array.

The locations of the steering beam spots on the photodiodes are controlled in the steering leg of the time delay controller in such a way as to maintain the required proportionality relationship between time delays. A single-channel steering Bragg cell driven with a steering tone is followed in the steering leg by angle amplification optics. The purpose of the angle amplification optics is to map the single beam out of the steering Bragg cell into multiple beams

having a range of locations on the photodiodes to generate the desired range of time delays. The result is that the locations of the steering beam spots on the photodiodes, and therefore the set of time delays, is controlled by the frequency of the single steering signal and by the angle amplification optics in the beam steering leg.

2.2 Architecture for Linear Receiving Arrays

Figure 4 shows an architecture to achieve true time delay beamforming for a receiving array. In order to form a beam in a particular direction with a receiving linear RF array, the outputs of the array elements are delayed relative to one another and then summed. The amount of relative delay between array elements is determined by the spacing between the array elements and by the angle between the beam and the normal to the array.

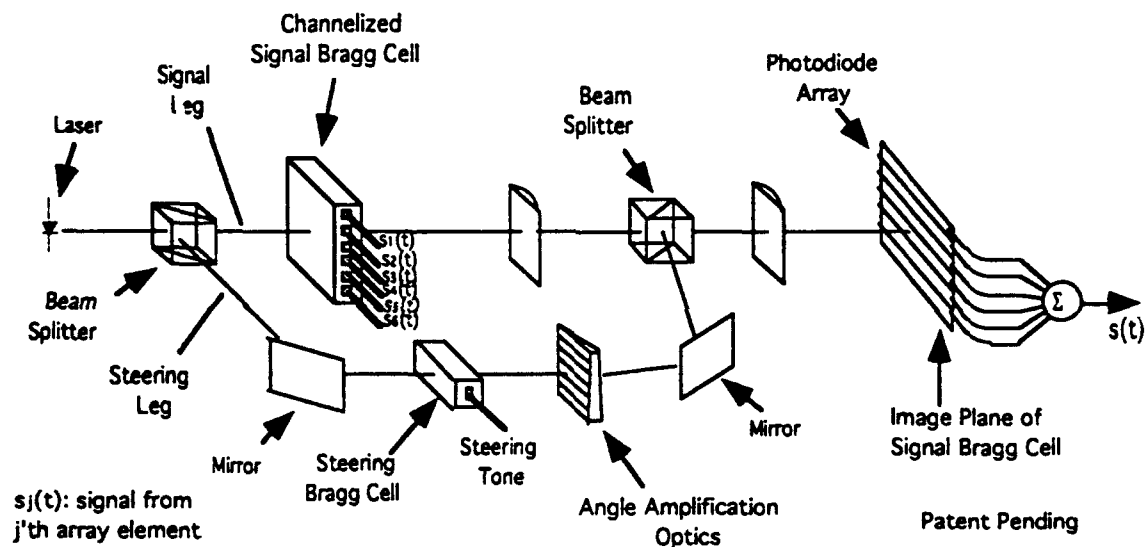


Figure 4. Architecture for a receiving array

The principle of how the architecture shown in Figure 4 for a receiving array delays a signal is the same as for the architecture for the transmitting array shown in Figure 2. In the case of a receiving array, a multi-channel Bragg cell is used in the signal leg of the interferometer, with the number of channels equal to the number of antenna elements or subarrays in the linear array. Here, an electrical signal from each element or subarray of the receiving array drives a channel of the multi-channel signal Bragg cell. The signal in each channel is imaged onto a corresponding photodiode in the array of photodiodes. As described above, the electrical output of a photodiode is a time delayed replica of the electrical signal that drives the corresponding channel of the multi-channel signal Bragg cell. The time delay is determined by the location of the steering beam spot on the face of the photodiode.

The steering leg of the interferometer in Figure 4 functions identically to the steering leg in the transmitting architecture shown in Figure 2. The angle amplification optics in the steering leg result in steering beam spots having a distribution of locations on the array of photodiodes. This allows a single-channel Bragg cell, driven with a tone to control a range of time delays.

The electrical outputs of the photodiodes are summed together to generate the desired signal. This sum forms a replica of the signal arriving at the linear antenna array from the direction determined by the frequency of the steering signal.

3. Steering Planar Arrays

The acousto-optic controllers for transmitting and receiving arrays described in Section 2 can be used for steering planar arrays. A planar array of array elements (or sub-arrays) is depicted in Figure 5. This figure defines the orientation of a beam formed by this array in terms of angle from the normal to the array (θ) and orientation of the projection of the beam onto the face of the array (azimuth angle ϕ).

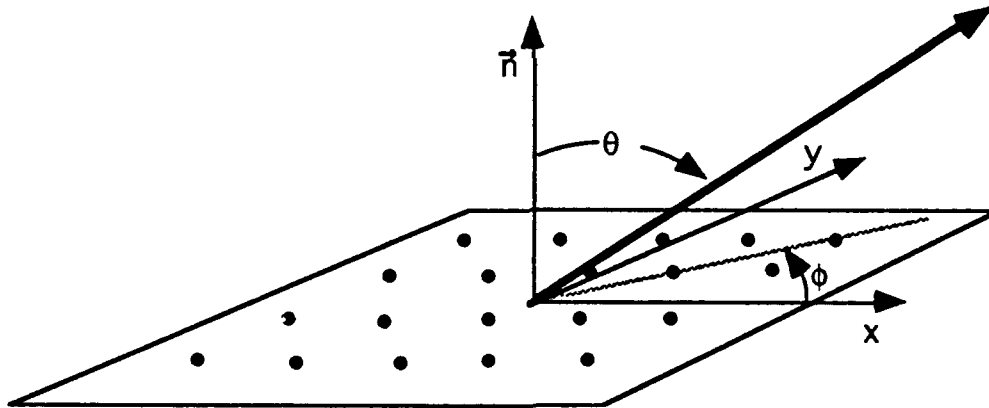


Figure 5. Planar array

If the array elements (centers of sub-arrays) are on a rectangular grid at locations (x_i, y_j) , then the time delays required to array element ij at position (x_i, y_j) to form a beam in the desired direction is given by the following equation:

$$\tau_{ij} = \frac{x_i}{c} \sin(\theta) \cos(\phi) + \frac{y_j}{c} \sin(\theta) \sin(\phi). \quad (9)$$

As indicated by Equation (9), the time delays are separable into a row component (x-component) and a column component (y-component). Therefore, the same controllers used to steer linear arrays can be cascaded together as shown in Figure 6 to steer a planar transmitting array. The number of time-delay control modules required to steer an $N \times N$ array is $N+1$: one controller to generate the N x-component delays, and N y-component controllers. The y-component delay controllers are identical to one another. Only two control signals are required: one for the x-component controller and one for all of the y-component controllers.

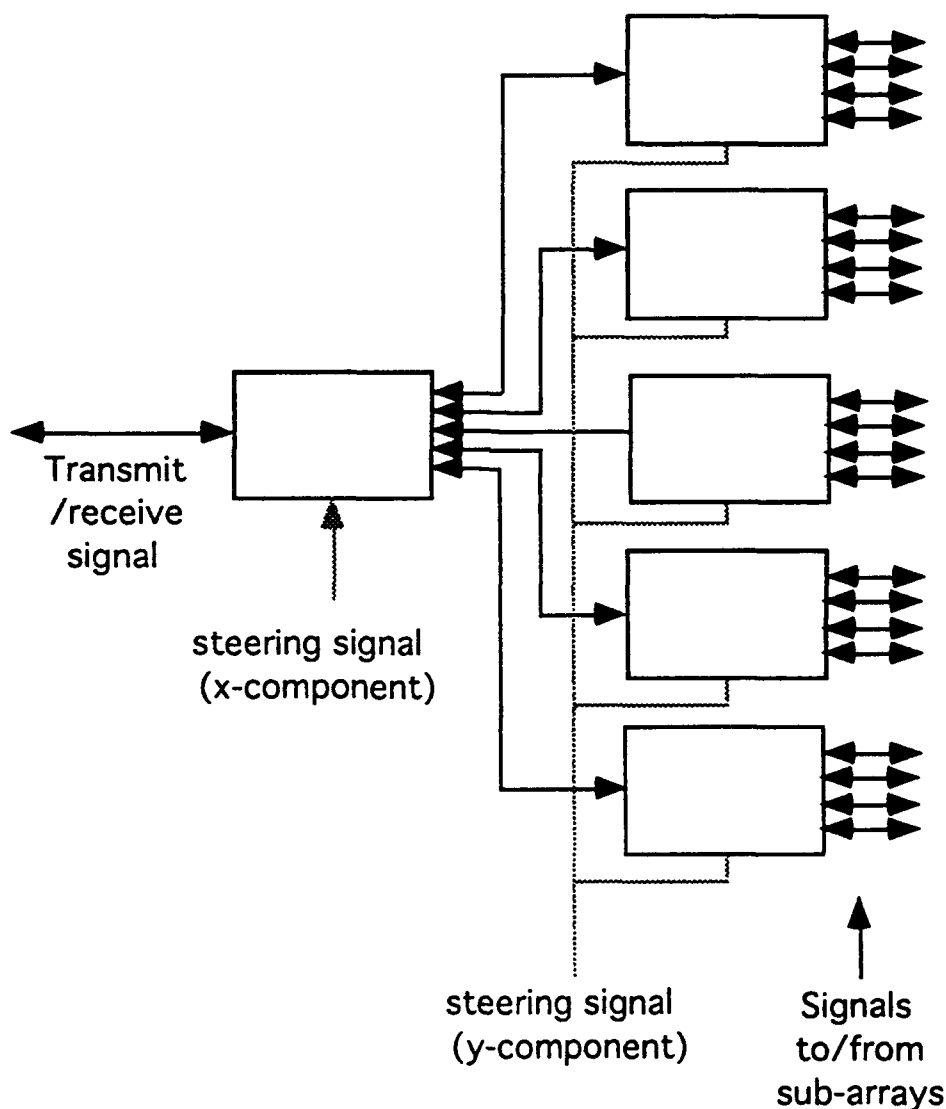


Figure 6. Cascading of time delay controllers to steer a planar array

4. TECHNICAL CONSIDERATIONS

4.1. Removal of Steering Signal Doppler Shift

The steering tone driving the steering Bragg cell results in a frequency shift of the optic steering beam by an amount equal to the frequency of the steering tone. The frequency shifted steering beam results in frequency shifts of the electrical signals out of the photodiodes. If this frequency shift is not acceptable, then this Doppler shift can be removed when converting between the IF of the time delay controller and the RF of the array as shown in Figure 7.

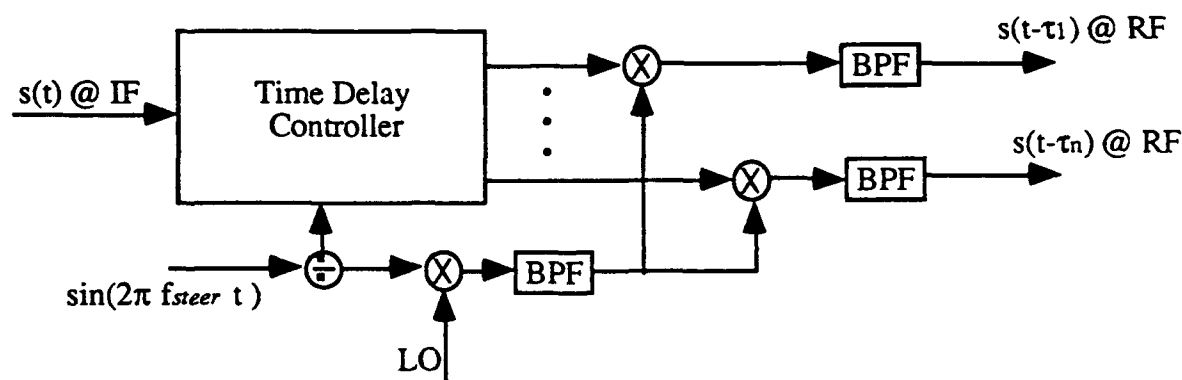


Figure 7. Removal of steering signal Doppler

4.2 Relationship Between Phases

In addition to providing the correct delay of the envelope of the wideband signal from one RF array element to the next, the time delay controller correctly and precisely shifts the phases of the carriers of the time delayed signals within a tight tolerance in order to form a beam in the desired direction at RF.

4.2.1 Providing Correct Phases at RF

Time delaying a signal at an IF frequency results in a carrier phase shift that would be correct if the signal were to be transmitted at that IF frequency, but is not correct after translating the signal up to its transmitted RF frequency. Because of this, an additional phase shift of each time delayed signal is required. For a delay τ , the phase shift adjustment that must be provided is given by

$$\Delta\phi = 2\pi \cdot \tau \cdot (RF - IF) . \quad (10)$$

If this additional phase adjustment is not made, then the time delayed envelope of the signal and the phase front of the carrier of the signal will attempt to form beams in different directions, resulting in beam broadening.

The phase shift adjustment given by Equation (10) is implemented by placing a transparent wedge in a Fourier plane of the steering Bragg cell of the time delay controller, as shown in Figure 8. The Fourier plane chosen is after the angle amplification optics. The taper and orientation of the wedge and its index of refraction determine the phase shift adjustment as a function of time delay.

The reason the wedge provides the required phase shift given by Equation (10) is as follows. Since both the photodiode array and the phase adjustment wedge are in Fourier planes of the steering Bragg cell, the photodiode array is in an image plane of the phase adjustment wedge. Therefore, the steering beam for each photodiode will be focused to a narrow spot in the wedge as well as on the detector. The lateral (horizontal) location of a focused steering beam spot is proportional to time delay.

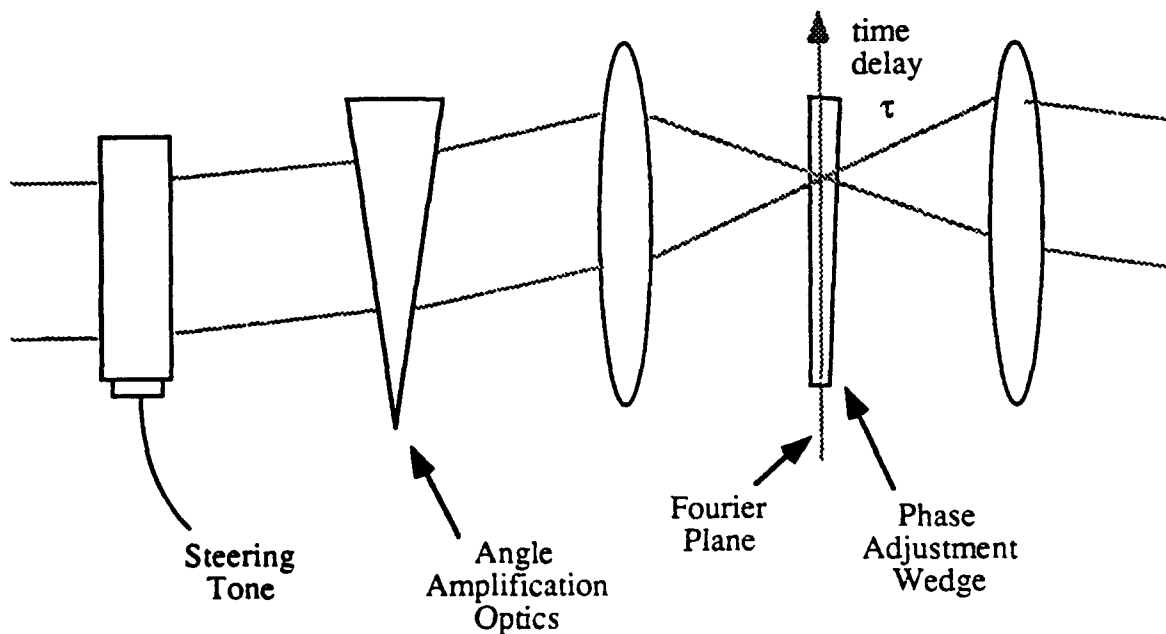


Figure 8. Use of wedge to provide time delay dependent phase adjustment

As the steering beam passes through the wedge, it will be differentially phase shifted by the amount

$$\Delta\phi = x \cdot (n - 1), \quad (11)$$

where x is the thickness of the wedge at the steering beam location and n is the index of refraction of the wedge material. For a wedge with planar faces, wedge thickness, x , is proportional to lateral position along the wedge, and therefore proportional to time delay on the photodiode array. So, for a wedge with planar surfaces, the phase shift adjustment provided by the wedge is proportional to the time delay as required by Equation (10).

4.2.2 Providing Phases with Small Uncertainties

There are two contributors to variations of phases from their ideal values: time independent contributions and time varying contributions. Time independent or fixed contributions to phase variations are due primarily to non-perfect optical components in the time delay controller. It should be possible to design and fabricate the time delay controller to have fixed phase variations from ideal relative phases of 18 degrees or smaller. Temporal variations of relative phases are expected to be a small fraction of the fixed phase variations. This is due in part to the fact that variations between the optical path lengths of the two legs of the interferometer will result in the same phase shift on each of the delayed signals and therefore will not cause the phase differences to vary. It is the phase differences that are important for beam forming and steering, not the absolute phases.

5. PROOF-OF-PRINCIPLE DEMONSTRATION

This section describes the results that were obtained from the proof-of-principle breadboard demonstration of the time delay controller. Figure 9 shows a schematic representation of the breadboard system, an implementation of the acousto-optic time delay controller architecture described in Section 2.1 above. The primary objective of this breadboard is to demonstrate the ability to finely control time delays, and to show that time delays are proportional to the frequency of the steering tone. As shown in Figure 9, two time-delayed signals are generated by the optical system to demonstrate true time delay.

The optical system is a Mach-Zehnder interferometer in which a beam from a coherent diode laser is split into the two legs, the signal leg and the steering leg, of the interferometer. Optical functions are performed in each leg, and then the beam is recombined by a second beamsplitter to form an interference pattern on a photodiode array.

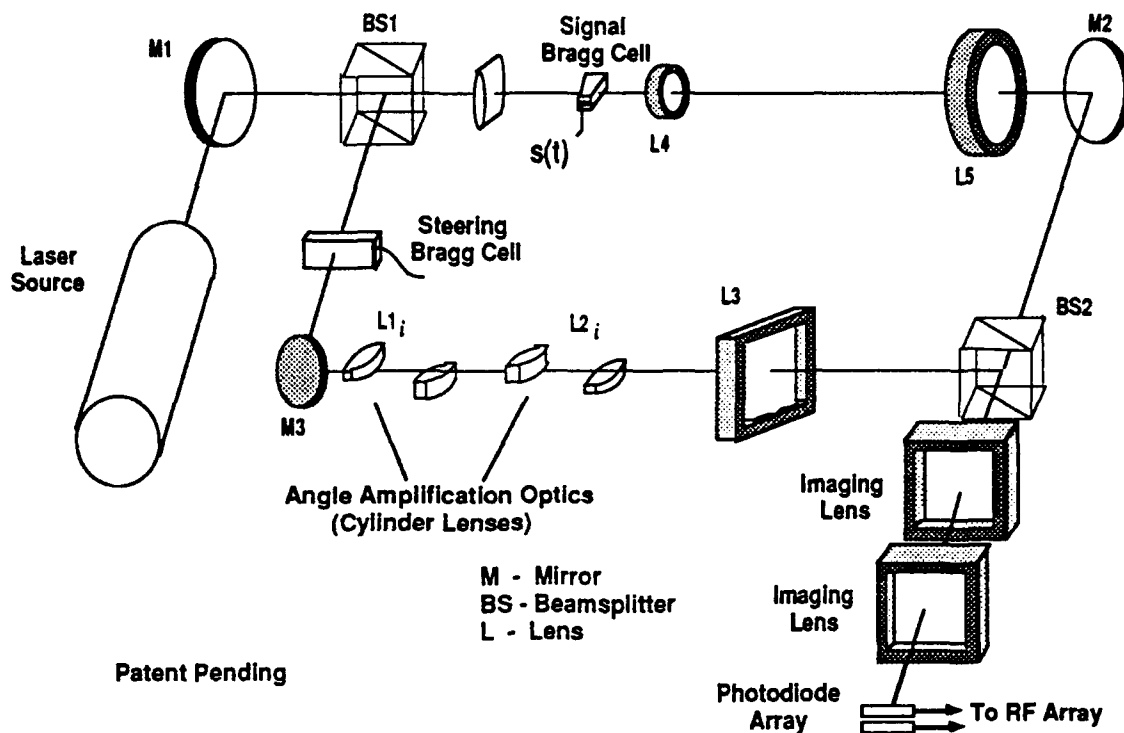


Figure 9. Proof-of-principle breadboard

The Bragg cell used in the signal leg is a gallium phosphide longitudinal mode (GaP-L) crystal with a diffraction bandwidth of 80 MHz centered at 200 MHz. The steering leg contains a tellurium dioxide (TeO₂) slow shear mode steering Bragg cell. The steering cell has a 10μsec aperture and a diffraction bandwidth of 8 MHz centered at 50 MHz. Two sets of cylinder lenses in the steering leg are used to perform the angle amplification to generate the two time-delayed output signals. The output signals are generated by detecting the interference of each steering beam with the signal beam on an avalanche photodiode (APD) array.

For the demonstration, the wideband signal was simulated by stepping narrowband tones sequentially across the full 80 MHz bandwidth of the signal Bragg cell. The time delays between the two output signals were determined for each of a set of steering frequencies by measuring the phase difference between the two delayed signals as a function of signal frequency. The time delay between the two delayed signals is equal to the slope of the phase difference between the two delayed signals versus signal frequency. Figure 10 shows a plot of phase versus signal frequency for a steering frequency of 49.5 MHz. From the slope of this plot, the relative time delay between the two outputs is estimated to be 1.73 nsec.

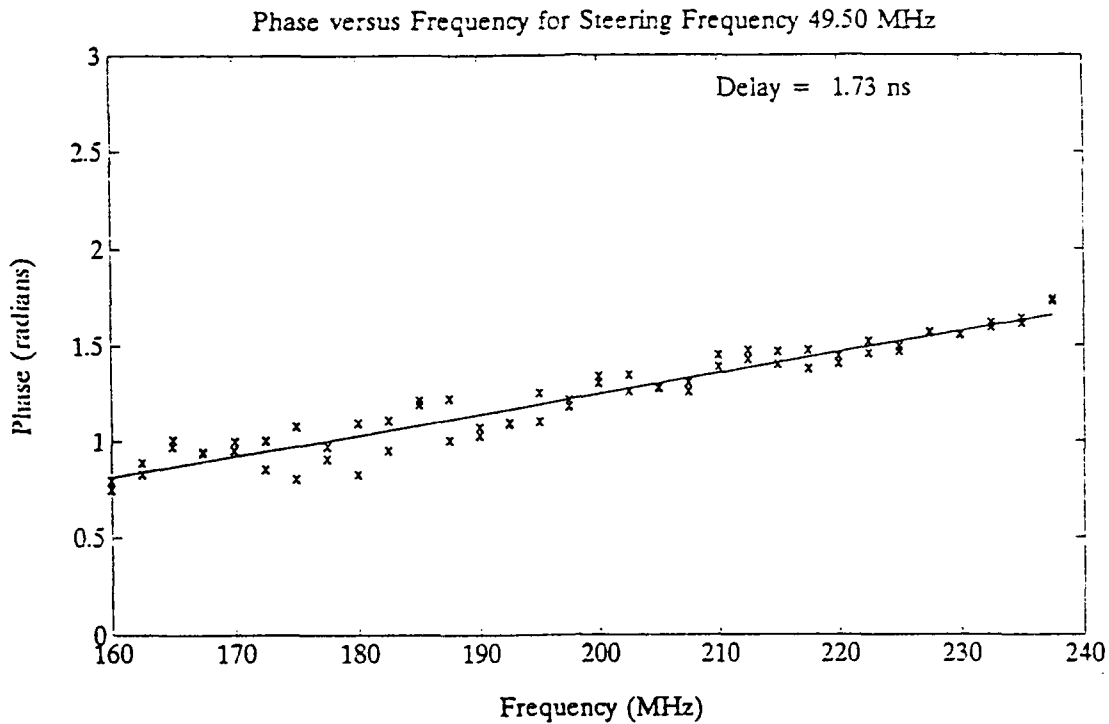


Figure 10. Phase difference versus signal frequency for a steering frequency of 49.5 MHz

The phase measurements shown in Figure 10 are for two scans of signal frequency so that there were two phase difference measurements taken at each signal frequency at well separated times. The rms error of the fit of the phase difference versus signal frequency to a straight line is 8 degrees. The spread of the data is due to both fixed system errors and long term drift in the measurement electronics. Both of these can be minimized in a rigorous engineering design. Figure 10 also shows a small deterministic deviation from a straight line fit. This pattern is also present at other steering frequencies. This deviation from straight line fit is probably due to some combination of defects in the optical and electronic system.

Phase difference versus signal frequency data was collected for a set of steering frequencies and time delays were estimated. Figure 11 shows a plot of the estimates of time delay versus steering frequency. As desired, the relationship between steering frequency and time delay is linear, with an rms deviation of 74 ps. From the slope, one sees that the sensitivity of time delay to frequency of the steering signal is 1.047 ps/kHz; thus, precise and stable steering should be easily maintainable with very moderate steering tone frequency synthesis requirements.

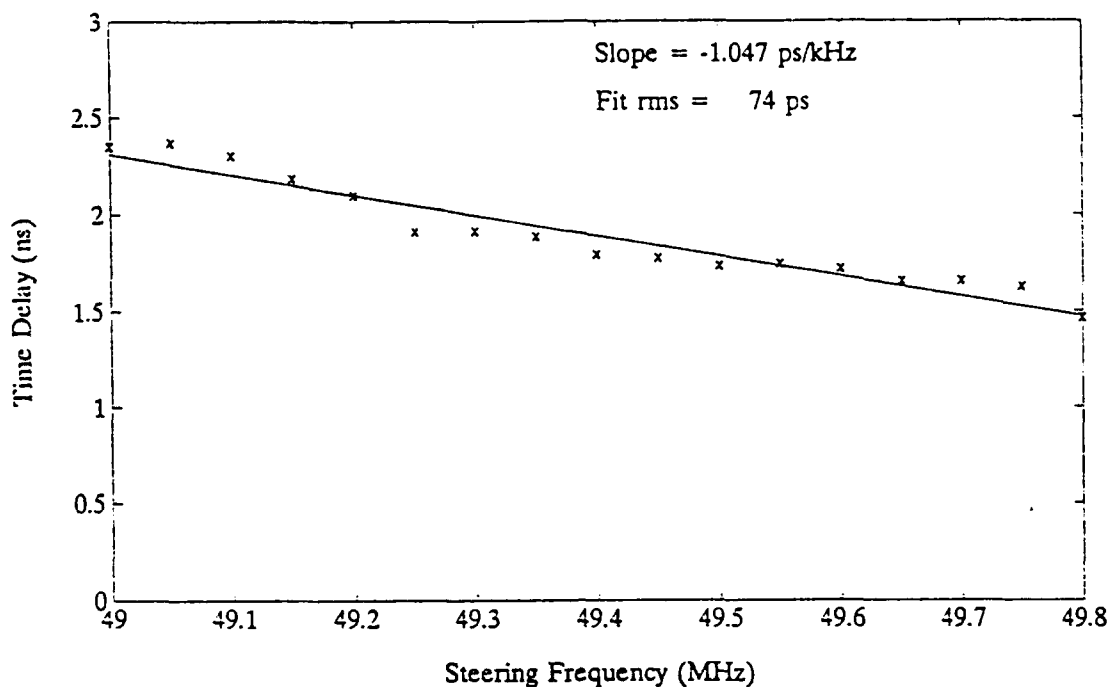


Figure 11. Time delay versus frequency of the steering signal

The spread of the data about the straight line fit appears to be predominantly due to fixed system errors, but additional testing would be required to exactly differentiate between the fixed system errors and long term drift of the measurement electronics. It is expected that in subsequent implementations of the acousto-optic time delay controller the rms error of the linear fit of the time delays to steering frequency will be reduced to less than 10 ps. The breadboard was designed to demonstrate proof-of-principle, not proof-of-performance. Demonstrating proof-of-principle did not require a rigorous optical design. Only simple, off-the-shelf lenses were used in the breadboard, and the design and assembly of the measuring electronics was simplistic. As a result, imperfections in the breadboard system combined to give phase difference versus signal frequency measurements and estimates of time delay versus steering frequency that do not fall perfectly on a straight line. Rigorous design and fabrication methods can correct these problems.

6. REALIZABILITY FOR REAL APPLICATIONS

Design parameters were computed for a set of strawman requirements corresponding to an array scanning the beam of a wideband signal over a large field of view. The purpose of this exercise is to show the feasibility of building an acousto-optic true time delay beamformer for real applications. The set of strawman requirements are:

Signal bandwidth	1 GHz,
Array RF	10 GHz,
Maximum steering angle	$\pm 60^\circ$,
Array length	2 m.

A set of acousto-optic design parameters that are realizable were found that satisfy the strawman design requirements. These include reasonable focal lengths and F-numbers of lenses, avalanche photodiodes of sufficiently high bandwidth and wide enough active area for the range of time delays required, and modest requirements for the signal and steering Bragg cells. For example, the requirements on the wideband signal Bragg cell are:

Bandwidth	1 GHz,
Time aperture	11.5 ns,
BT product	11.5.

The minimum allowed time-bandwidth product of the steering Bragg cell is simply 4 times the time aperture of the signal Bragg cell times the maximum frequency of the wideband signal within the time delay controller. The requirements on the steering Bragg cell parameters are:

Bandwidth	10 MHz,
Time aperture	11.6 μ s,
BT product	116.

The steering signal bandwidth of 10 MHz means that it is easy to control the steering of the beam over ± 60 degrees to very fine pointing angles. For example, changing steering frequency by 83 kHz changes the pointing angle of the beam by .1 degrees.

7. CONCLUSIONS

The acousto-optic architecture described in this report is ideally suited for true time delay control of transmitting/receiving arrays. The demonstration of the proof-of-principle breadboard shows that the time delays of a signal can be precisely controlled with a single steering tone, and that the relationship between time delays (pointing direction of the RF array) and the frequency of the steering tone is linear. For the particular design parameters of the breadboard, the sensitivity of time delay to frequency of the steering tone was measured to be 1.05 ps/kHz; therefore, the frequency of the steering tone need only be controlled to a few kHz to precisely control the time delays and, therefore, the pointing direction of an array.

The next phase in the development of the acousto-optic true time delay beam controller needs to be the development and demonstration of a proof-of-performance model. This model would demonstrate the generation and control of the number of time delays at wide bandwidth that would be required to steer a specific array and demonstrate high SNR performance.

8. REFERENCES

1. I. C. Chang and S. S. Tarnq, "Phased array beamforming using acousto-optic techniques", *Proc. SPIE*, vol. 936, pp. 163-167, 1988.
2. D. Dolfi, F. Michel-Gabriel, S. Bann, and J. P. Huignard, "Two-dimensional optical architecture for time-delay beam forming in a phased-array antenna," *Optics Letters*, vol. 16, pp. 255-257, February 1991.
3. G. A. Koepf, "Optical processor for phased-array antenna beam formation," *Proc. SPIE*, vol. 477, pp. 75-81, 1984.
4. K. A. Nickerson, P. E. Jessop, and S. Haykin, "Optical processor for array antenna beam shaping and steering," *Optical Engineering*, vol. 30, pp. 1497-1502, October 1991.
5. N. A. Riza and D. Psaltis, "Acousto-optic signal processors for transmission and reception of phased-array antenna signals," *Applied Optics*, vol. 30, pp. 3294-3303, August 1991.
6. N. A. Riza, "A transmit/receive time delay optical beamforming architecture for phased array antennas," *Applied Optics*, vol. 30, pp. 4594-4595, November 1991.
7. N.A.Riza "An acoustooptic phased array antenna beamformer with independent phase and carrier control using single sideband signals," *IEEE Photonics Technology Letters*, vol. 4, pp. 177-179, February 1992.

8. N. A. Riza "Acousto-optic architecture for two-dimensional beam scanning in phased-array antennas," *Applied Optics*, vol. 31, pp. 3278-3284, June 1992.
9. N. A. Riza "An acoustooptic-phased-array antenna beamformer for multiple simultaneous beam generation," *IEEE Photonics Technology Letters*, vol. 4, pp. 807-809, July 1992.
10. E. N. Toughlin, H. Zmuda, and P. Kornreich, "A deformable mirror-based optical beamforming system for phased array antennas," *IEEE Photonics Technology Letters*, vol. 2, pp. 444-446, June 1990.
11. R. T. Weverka, K. Wagner, and A. Sarto, "Optical processing for self-cohering of phased-array imaging radars," *Proc. SPIE*, vol. 1703, pp 552, 1992.
12. L. H. Gesell and J. L. Lafuse, "True time delay beam formation," U.S. Patent No. 5,202,776, issued April, 1993.
13. L. H. Gesell and T. M. Turpin, "True time delay beam forming using acousto-optics," *Proc. SPIE*, vol. 1703, 1992.
14. L. H. Gesell and T. M. Turpin, "Time delay beam formation," U.S. Patent Application No. 08/045,062, April, 1993.

APPENDIX A

True Time Delay Beamforming

Annual Status Report

TABLE OF CONTENTS

	PAGE
ABSTRACT.....	1
1. INTRODUCTION	2
1.1 Identification and Significance of the Problem	2
1.2 Project Objectives.....	3
1.2.1 Task 1: Feasibility Analysis	4
1.2.2 Task 2: Proof-of-Principle Demonstration.....	4
1.3 Status and Accomplishments	4
1.4 Strawman Design Parameters and Associated Risks	6
1.5 Future Development Phases.....	6
2. INTRODUCTION OF PRINCIPLES	7
2.1 Spectral Domain View of Beamforming	7
2.2 When True Time Delay Beamforming is Needed	8
2.3 Principle of Generating Time Delays	10
2.3.1 Frequency Domain	10
2.3.2 Time Domain.....	14
3. ARCHITECTURES	16
3.1 Processor Structures versus Operational Modes	16
3.2 Fourier Plane Architecture for Linear Transmitting Arrays	17
3.3 Architectures for Linear Receiving Arrays.....	19
3.4 Multiple Beam Capabilities	21

TABLE OF CONTENTS
(continued)

	PAGE
3.5 Single- versus Multi-Element Modules and Single- versus Multiple-Signals.....	21
3.6 Planar Arrays.....	25
4. ANALYSIS OF TECHNICAL ISSUES	26
4.1 Angle Amplification	26
4.1.1 With Prisms.....	26
4.1.2 With Lenses.....	29
4.1.3 Recommendation.....	31
4.2 Carrier Phase Adjustment for IF to RF Translation.....	31
4.3 Photodiode Considerations	32
4.4 RF Array Sidelobes.....	33
5. DEMONSTRATION BREADBOARD	39
5.1 Strawman Requirements and Constraints.....	39
5.2 Breadboard Architecture Selection.....	40
5.3 Breadboard Design	40
5.3.1 Parametric Relationships for Selecting Lens and Bragg Cell Parameters.....	41
5.3.2 Example Lens and Bragg Cell Parameter Values	52
5.3.3 Phase Adjustment Wedge Parameters.....	53
5.4 Optical Efficiency, Detector Characteristic, and SNR	56

TABLE OF CONTENTS
(continued)

	PAGE
5.5 Scan Angle Sensitivity.....	62
5.5.1 No Angle Amplification	63
5.5.2 Angle Amplification with Lenses.....	64
6. SUMMARY OF ANALYSIS.....	65
6.1 Beamwidth.....	65
6.2 FM Spreading.....	65
6.3 Sidelobes.....	66
6.4 Number of Simultaneous Beams.....	66
6.5 Scaling to Large Arrays.....	67
6.6 Beam Scanning Rate.....	67
6.7 Beam Scan Accuracy, Range.....	68
6.8 Signal Fidelity.....	68
6.9 Signal-to-Noise	69
6.10 RF Bandwidth.....	69
6.11 Translation from IF to RF	69
6.12 RF/Beam Direction Dependence	70
7. RECOMMENDATIONS	71
7.1 Recommend Breadboard Demonstration.....	72
7.2 Final Recommendations.....	72
8. REFERENCES.....	73

LIST OF FIGURES

	PAGE
Figure 1-1. Work Plan.....	3
Figure 2-1. Beam Dispersion with Frequency Independent Phase Shifts	8
Figure 2-2. Signal Bandwidth Threshold versus Array Length for True Time Delay Beamforming	9
Figure 2-3. Beamwidth Threshold versus Fractional Bandwidth for True Time Delay Beamforming.....	10
Figure 2-4. Simplified Fourier Plane Architecture to Delay a Signal.....	11
Figure 2-5. Reference Plane Wave and Signal Spectrum on the Photodiode	11
Figure 2-6. Simplified Image Plane Architecture to Delay a Signal	14
Figure 2-7. Tapping the Signal Bragg Cell on the Photodiode	15
Figure 3-1. Fourier Plane Architecture for a Transmitting Linear Array.....	17
Figure 3-2. Fourier Plane Architecture of a Receiving Linear Array.....	20
Figure 3-3. Image Plane Version of a Single-Element Module Architecture	22
Figure 3-4. Transmitting Multiple Signals Using One Multi-Element Module.....	23
Figure 3-5. Transmitting a Single Signal Using Single-Element Modules	23
Figure 3-6. Transmitting Multiple Signals Using a Multi-Element Module for Each Signal.....	24
Figure 3-7. Transmitting Multiple Signals Using a Single-Element Modules.....	24
Figure 3-8. Mapping of Set of Time Delays to a Planar Array.....	25
Figure 4-1. Angles for Describing Bragg Cell/Prism Optical Beam Control.....	27
Figure 4-2. Output Angle from Prism versus Input Angle for Five Different Prisms Wedge Angles	28
Figure 4-3. Angle Amplification versus Input Angle for Five Different Prism Wedge Angles	29

LIST OF FIGURES
(continued)

	PAGE
Figure 4-4. Pair of Concave Lens for Angle Amplification	30
Figure 4-5. Use of Wedge to Provide Time Delay Dependent Phase Adjustment.....	32
Figure 4-6. Reference Beams with its Sidelobes on the Photodiode.....	34
Figure 4-7. Generation of RF Array Sidelobes from the Spurious Time Delays	35
Figure 4-8. Generation of Echoes from the Spurious Time Delays	36
Figure 4-9. Relative Spot Size of Steering Beam versus Sidelobe Level.....	37
Figure 4-10. Truncation Ratio (in Units of 1/e Points) as a Function of.....	38
Figure 5-1. Optical Layout for the Demonstration Breadboard	41
Figure 5-2. Steering Leg of the Time Delay Processor	43
Figure 5-3. Signal Leg of the Time Delay Processor	44
Figure 5-4. System signal-to-noise ratio as a function of beamsplitting ratio.....	61
Figure 5-5. Signal-to-noise ration as a function of gain in an APD	62
Figure 5-6. Beam Scan Angle versus Steering Control Frequency for no Angle Amplification	63
Figure 5-7. Beam Scan Angle versus Steering Control Frequency	64

ABSTRACT

Wide aperture arrays for transmitting and receiving wideband signals suffer beam broadening when steered away from the array normal using phase delays between the array elements. This beam dispersion is eliminated if time delays instead of phase shifts are used between antenna array elements. This report describes the progress of a project to develop and demonstrate an acousto-optic signal processing concept that generates and controls, with a single control signal, the set of time delays required for linear antenna array beamforming. This acousto-optic architecture allows an array to scan a beam rapidly over a continuum of angles.

In the approach described in this report, the time delays between elements are generated by using an acousto-optic (AO) Bragg cell as a continuous delay line, and optically tapping selected points in the Bragg cell to the output. This optical tapping is controlled with a second Bragg cell and other standard passive optical elements. Included in this concept is a passive optical element to ensure that the phase shifts of the carrier of the time delayed signals will be correct at the RF of the array.

Section 1

INTRODUCTION

1.1 Identification and Significance of the Problem

Wide aperture, wide bandwidth phase steered array antennas suffer beam broadening when steered away from the array normal. Using time delays rather than phase delays between the array elements eliminates this problem of beam dispersion. A brute force approach for implementing true time delay beamforming is to switch in different lengths of signal transmission delay lines between the common signal source and the antenna array elements; however, this approach can be bulky and cumbersome for scanning an array with a large number of elements over a wide range of nearly continuous angles.

A number of investigators¹⁻¹¹ have proposed using optical signal processing technologies for both phase and time delay beamforming. This report describes a Rome Laboratory funded project being conducted by Essex to demonstrate the proof-of-principle of an acousto-optic architecture to generate and rapidly change the time delays of a signal for true time delay beamforming and steering. The Essex approach is to use an acousto-optic Bragg cell as a delay line and to use a second steering Bragg cell to control the points in the signal delay line Bragg cell that are tapped to the output. This approach allows a beam to be rapidly scanned over a continuum of angles by changing the frequency of a single tone that drives the steering Bragg cell in this architecture^{12,13}. Multiple beams can be simultaneously scanned if a multi-frequency steering signal is used. This architecture is simple and does not lead to a bulky and complex implementation: the required hardware can fit into a small, light-weight package, be rugged, and consume a small amount of power. The simplicity and compactness of the architecture dramatically reduces unwanted variability in the time delays.

There are two variants of the acousto-optic time delay architecture: a frequency-domain and a time-domain version. These two variants of the architecture are based on application of an acousto-optic interferometric spectrum analyzer architecture¹⁴ to interference excision^{15,16}. The spectral domain view of phased array beamforming is first reviewed in Section 2 and the principles of how the frequency-domain and time-domain variants of the architecture to generate time delays are described. Section 3 presents acousto-optic architectures for generating and controlling a set of time delays for transmitting and receiving arrays. Section 4

presents the analysis of several key technical issues in the implementation of the beamforming processor, and Section 5 describes the choice of design parameters for the demonstration breadboard and the expected performance in terms of such parameters as signal-to-noise ratio, processor, and scan angle sensitivity. Section 6 summarizes the results of the performance analysis study, and Section 7 presents a conclusions in terms of architectural choices.

1.2 Project Objectives

The objectives of this project are to investigate and validate the feasibility, and to determine the advantages and limits, of using acousto-optic signal processing concepts for true time delay beamforming and steering. These objectives are being accomplished through analysis (Task 1) and laboratory demonstration (Task 2). The workplan for accomplishing these objectives is shown in Figure 1-1.

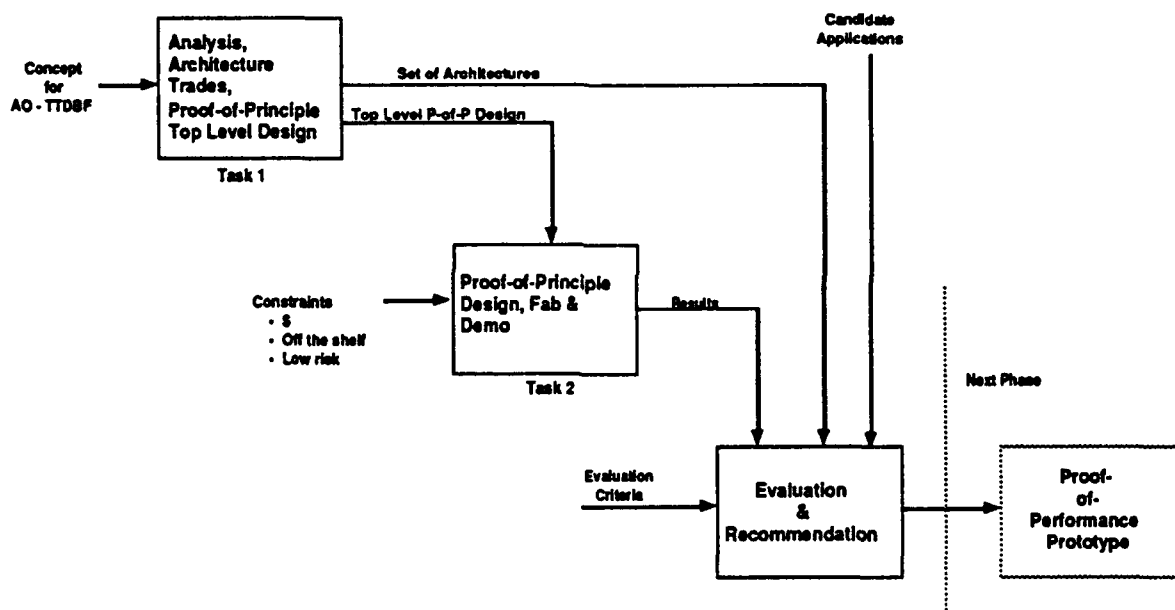


Figure 1-1. Work Plan

1.2.1 Task 1: Feasibility Analysis

The purpose of the feasibility analysis task is to gain an understanding of how each of the architectures generates and controls the time delays and to establish the parametric relationships between the beamforming performance parameters and the architecture design and implementing hardware parameters, and to perform a top level design of a feasibility unit to be demonstrated in Task 2.

1.2.2 Task 2: Proof-of-Principle Demonstration

The purpose of this task is to demonstrate the proof-of-principle of the proposed acousto-optic true time delay beamforming approach. This unit will be demonstrated in the laboratory at Essex.

In addition to showing feasibility, this model will be used as an experimental apparatus to explore performance ranges and limits of the selected approach. Performance will be compared with results expected from the analytical analysis performed in Task 1.

Information will be gathered and experience gained to guide the design of a proof-of-performance model, and to intelligently trade (objectively and subjectively) the demonstrated method with other methods of true time delay beamforming.

1.3 Status and Accomplishments

Feasibility analysis (Task 1) has been completed and Task 2 to perform a proof-of-principle of the selected true time delay beamforming architecture is well under way.

Alternative acousto-optic processing architectures for true time delay beamforming were identified and defined. Included are architectures for transmitting and receiving, using one- and two-dimensional arrays.

A trade study of the performance of the candidate architectures was carried out. Examples of performance parameters and issues that were considered in this trade analysis are the following:

- Effects of the time delay generation on signal fidelity, signal-to-noise, beamwidth and sidelobes;

- The number of multiple beams that can be generated simultaneously;

The effect of multiple simultaneous beams;
Beam scanning accuracy, rate, and range;
RF range and bandwidth;
Translating signals delayed at IF to RF;
Array size limitations, if any, and the ability to scale to large arrays;
FM spreading.

Based on this analysis, an architecture is recommended for each of the application conditions: size of array, one-dimensional versus two-dimensional arrays, transmitting versus receiving.

A configuration was recommended for a laboratory unit to demonstrate the feasibility of the principle of the proposed acousto-optic true time delay beamforming approach. A top level design of this demonstration unit was developed.

On Task 2, the detailed design of the of the proof-of-performance breadboard was completed and hardware is being procured. All hardware components are expected to be received by the end of March, 1993, at which time the unit will be assembled. After assembly, performance parameters of the unit will be investigated.

A small scale feasibility demonstration model, based on a specific architecture selected in Task 1, has been designed. Components for this unit are being procured. This unit will be and and demonstrated in the laboratory at Essex.

1.4 Strawman Design Parameters and Associated Risks

The nominal strawman design parameters chosen for the proof-of-principle demonstration are the following:

Signal bandwidth	1 GHz
IF	2 GHz
RF	> 2 GHz
Array Type	Linear
Array Length	2 meters
Scan range	± 60 degrees

The goal for the proof-of-principle demonstration is to generate and dynamically change a minimum of two simultaneous time delays.

The project budget limits hardware to off-the-shelf components where possible. Neither the time nor the money is available on this effort to design and procure the custom optical components that would provide for high optical efficiency of the breadboard. Therefore, performance, such as SNR, will be limited, but should be sufficient to demonstrate proof-of-principle.

1.5 Future Development Phases

Phase II: Engineering Model:

Design and build a proof-of-performance unit to demonstrate, in the laboratory, the full range of capabilities of the concept.

Phase III: Field Demonstration:

Demonstrate the engineering model with an antenna array.

Section 2

INTRODUCTION OF PRINCIPLES

The principles of true time delay beamforming are reviewed in this section. A spectral domain view of beamforming shows that to avoid beam dispersion each spectral component of the signal must be phase shifted by an amount that is proportional to frequency of that component. The principles of using acousto-optics to time delay a signal is then introduced. Both frequency and time domain acousto-optic interferometric architectures are considered.

2.1 Spectral Domain View of Beamforming

Figure 2-1 depicts the spread in beamwidth that occurs when transmitting a wideband signal with a phased array using frequency independent phase shifts. If the signal spans the frequency range from lower frequency f_1 to upper frequency f_2 , and all spectral components are phase shifted by ϕ , then the steering angles of the lowest and highest frequency components of the signal (α_1 and α_2 , respectively) are given by

$$\alpha_1 = \arcsin \left(\frac{\phi}{2\pi} \frac{c/f_1}{b} \right), \quad \alpha_2 = \arcsin \left(\frac{\phi}{2\pi} \frac{c/f_2}{b} \right) \quad (2.1)$$

where b is the separation between array elements and c is the velocity of light. From Equations (2.1), and as shown in Figure 2-1, the higher frequency components of the signal are steered closer to the normal of the array than are the lower frequency components when frequency independent phases are used.

The relations in Figure 2-1 above show that frequency dependent phase shifts are required to form a beam at an angle α , with the relationship between phase (ϕ), angle (α), and frequency (f) given by

$$\phi(f) = 2\pi f \frac{b \sin(\alpha)}{c} \quad (2.2)$$

Such frequency dependent phase shifts that vary linearly with frequency are, of course, equivalent to time delay τ , given by

$$\tau = \frac{b \sin(\alpha)}{c} \quad (2.3)$$

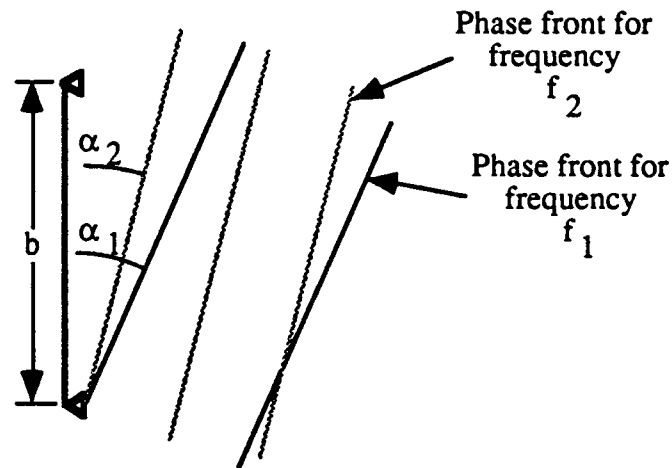


Figure 2-1. Beam Dispersion with Frequency Independent Phase Shifts

2.2 When True Time Delay Beamforming is Needed

In this section the conditions for when true time delay beamforming is required are reviewed. Figure 2-1 above depicts the beam dispersion that occurs when true time delay beamforming is not used when transmitting or receiving a wideband signal with an array. Equation (2.3) states the amount of delay between array elements that is required to form a beam at a desired angle with respect to the normal to the array. The discussions in Section 2.1 do not, however, indicate under what conditions true time delay beam steering is required versus when it is not required. In this section, it is seen that the requirements for true time delay beamforming are a function of parameters such as fractional bandwidth, scan angle, and desired beamwidth.

In order to form a beam in a particular direction using frequency independent phase shifts, that is without true time delays, the coherence time of the signal must be as long or longer than the difference in propagation time of the signal emitted from each of the array end elements. This time difference between two array elements separated by a distance b for a signal transmitted at an angle α from the array normal is given by Equation (2.3) above. The coherence time of a signal is the inverse of the bandwidth B of the signal. If this coherence time is less than the propagation time difference between array end elements, then true time delay beamforming must be used to avoid broadening of the beam. That is, true time delay beamforming must be used when the condition on the signal bandwidth is given by

$$B \geq \frac{c}{b} \frac{1}{\sin(\alpha)}; \quad (2.4)$$

where c is the speed of light.

Figure 2-2 is a plot of the threshold bandwidth versus array length, for beam pointing angles of 30 and 60 degrees, above which true time delay beamforming is required.

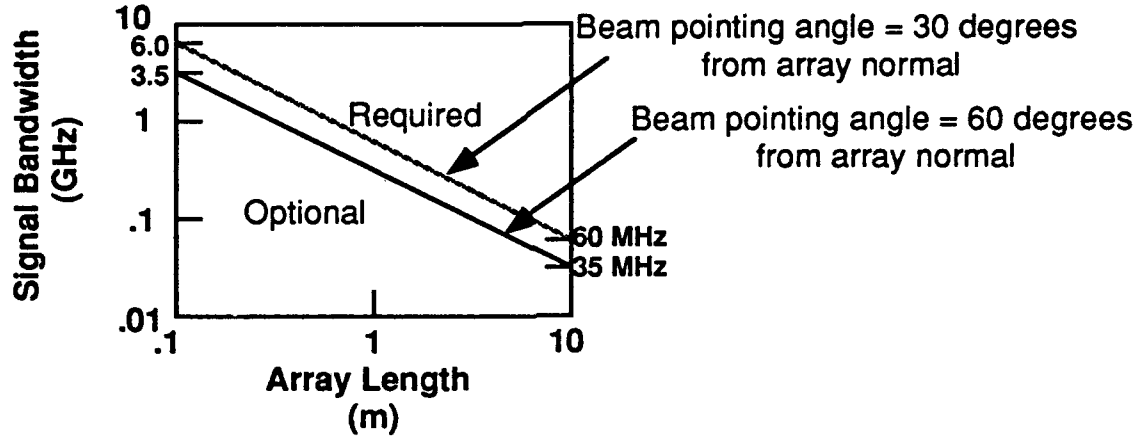


Figure 2-2. Signal Bandwidth Threshold versus Array Length for True Time Delay Beamforming

The requirement for true time delay beamforming can also be stated in terms of the fractional bandwidth of the signal and the beamwidth. The signal RF and the array length determine the angular width of the beam ($\delta\alpha$) formed by the array:

$$\delta\alpha = \frac{c}{b} \frac{1}{\text{RF}} \quad (2.5)$$

Inequality (2.4) and Equation (2.5) can be combined to eliminate the ratio c/b to obtain an expression for values of beamwidth below which true time delay beamforming is required:

$$\delta\alpha \leq \frac{B}{\text{RF}} \sin(\alpha) \quad (2.6)$$

This indicates that true time delay beamforming is required when the desired beamwidth, in radians, is less than the fractional bandwidth of the signal times the sine of the scan angle. Figure 2-3 is a plot of the threshold beamwidth versus fractional bandwidth of the signal, for beam pointing angles of 30 and 60 degrees, below which true time delay beamforming is required.

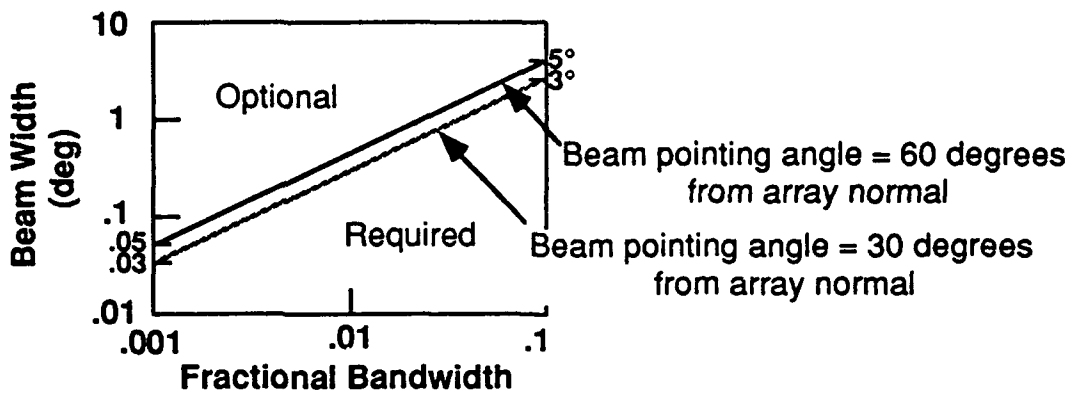


Figure 2-3. Beamwidth Threshold versus Fractional Bandwidth for True Time Delay Beamforming

2.3 Principle of Generating Time Delays

The time delays of a wideband signal are generated by using a wideband bulk acousto-optic Bragg cell as a delay line. A second Bragg cell is used to dynamically control which points in the signal Bragg cell are tapped to the output. There are two approaches for tapping the signal Bragg cell: a frequency-domain Fourier plane approach, and a time-domain image plane approach. This section defines and describes these two approaches for generating time delays.

2.3.1 Frequency Domain

This section explains how a time delayed replica of an electrical signal $s(t)$ is obtained from the photodiode in the frequency domain version of the acousto-optic true time delay architecture (Figure 2-4), and how this time delay is determined by the orientation of the optical reference beam at the photodiode. In the simplified architecture shown in Figure 2-4, only one delay is generated, with no means to dynamically change this delay.

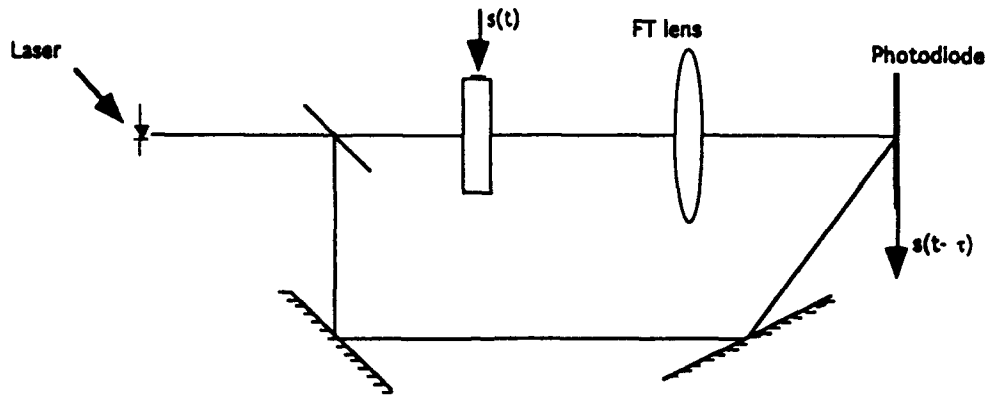


Figure 2-4. Simplified Fourier Plane Architecture to Delay a Signal

The optical reference beam traveling through the lower leg of the interferometric architecture in Figure 2-4 is a plane wave at the photodiode, making an angle of θ with the face of the photodiode (see Figure 2-5).

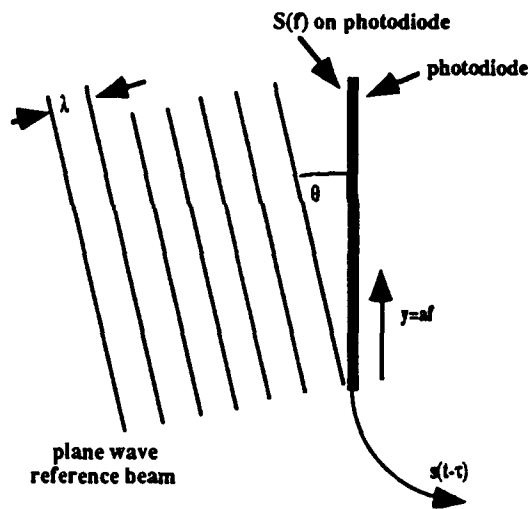


Figure 2-5. Reference Plane Wave and Signal Spectrum on the Photodiode

This reference plane wave at the photodiode is given mathematically by:

$$r(t,y) = e^{j2\pi (f_0 t - \frac{y}{\lambda} \sin \theta)} = e^{j2\pi f_0 (t - \frac{y}{c} \sin \theta)} \quad (2.7)$$

where t is time, y is the physical distance along the photodiode, λ is the optical wavelength of the reference beam, f_0 is the optical carrier frequency, and c is the velocity of light.

A coherent optical beam from the upper leg of the interferometer in Figure 2-4, modulated by the spectrum of the signal $s(t)$ and by tones oscillating at the spectral frequencies of $s(t)$, also illuminates the photodiode. This modulated coherent beam has the following functional form at the photodiode:

$$S(f) \cdot e^{j2\pi ft} e^{j2\pi f_0 t} \quad (2.8)$$

The oscillators

$$e^{j2\pi ft} \quad (2.9)$$

come from the fact that each spectral component of the signal in the acousto-optic Bragg cell Doppler shifts the optical carrier by the frequency of that spectral component.

Also, as depicted in Figure 2-5 and indicated in Equation (2.4), the phase of the reference plane wave on the photodiode varies linearly with distance along the photodiode. Since spectral frequency f in the Fourier transform plane (face of the photodiode) is proportional to the physical distance y along the photodiode, a factor τ can be defined such that

$$f\tau = -f_0 \frac{y}{c} \sin \theta, \text{ or } \tau = -\frac{y}{f} \frac{f_0}{c} \sin \theta \quad (2.10)$$

Note that τ is proportional to the sine of the angle between the reference plane wave and the photodiode. The reference wave at the photodiode (Equation (2.7)) can therefore be expressed as

$$r(t, f) = e^{j2\pi f\tau} e^{j2\pi f_0 t} \quad (2.11)$$

Square law detection on the photodiode results in multiplication of the signal spectrum by the reference plane wave, so that each spectral component is phase shifted by an amount proportional to the frequency of that component. This is equivalent to introducing a time delay. The output, $d(t)$, of the photodiode is this square-law detection at each instant of time, spatially integrated along the length of the photodiode, i.e., integrated with respect to frequency f . This can be stated mathematically as:

$$d(t) = \int \left| r(t, f) + S(f) \cdot e^{j2\pi ft} e^{j2\pi f_0 t} \right|^2 df \quad (2.12a)$$

$$= \int \left| e^{j2\pi f \tau} e^{j2\pi f_0 t} + S(f) \cdot e^{j2\pi ft} e^{j2\pi f_0 t} \right|^2 df \quad (2.12b)$$

$$= \text{bias} + 2 \operatorname{Re} \left[\int S(f) e^{j2\pi f(t-\tau)} df \right], \quad (2.12c)$$

where $\operatorname{Re}[\]$ denotes the real part of the complex quantity in the brackets.

Therefore, the detector output is

$$d(t) = \text{bias} + 2 \operatorname{Re} [s(t - \tau)]. \quad (2.13)$$

Since the input signal $s(t)$ driving the Bragg cell is real, the detector output is the input signal $s(t)$ on a bias delayed by time t . From Equation (2.10), the time delay τ is proportional to the sine of the angle of incidence of the reference plane wave on the photodiode. The bias allows negative and positive values of the delayed signal to be represented.

A more physical explanation of how the acousto-optic architecture shown in Figure 2-4 produces a delayed replica of the input signal, with the amount of delay determined by the orientation of the reference beam, is the following. Since the photodiode coherently sums all the spectral components of the signal $s(t)$, only those components of the spectrum that are in phase with one another, after being phase shifted by the reference signal, will lead to a nonzero output signal relative to the bias. Since the reference signal is a plane wave, the components of the signal spectrum, in optical form, that contribute to an output signal must also be a plane wave if, after being phase shifted by the reference signal, all points on the photodiode are to be at the same phase. Components of the optical signal that contribute to a plane wave in the Fourier plane (at the photodiode) come from a single point in the Bragg cell. The location of the point in the signal Bragg cell can be easily determined by considering the reference plane wave reflecting off the face of the detector array and propagating back through the Fourier transform lens. The location in the Bragg cell at which the reflected reference beam would be focused is the point in the signal Bragg cell that is tapped to the output. Thus, the reference wave selects which point in the signal Bragg cell (a delay line) is tapped to the output.

2.3.2 Time Domain

This section explains how a time delayed replica of an electrical signal $s(t)$ is obtained from the photodiode in the time domain version of the acousto-optic true time delay architecture (Figure 2-6), and how this time delay is determined by the location of the focused optical reference beam on the photodiode. In the simplified architecture shown in Figure 2-6, only one delay is generated, with no means to dynamically change this delay.

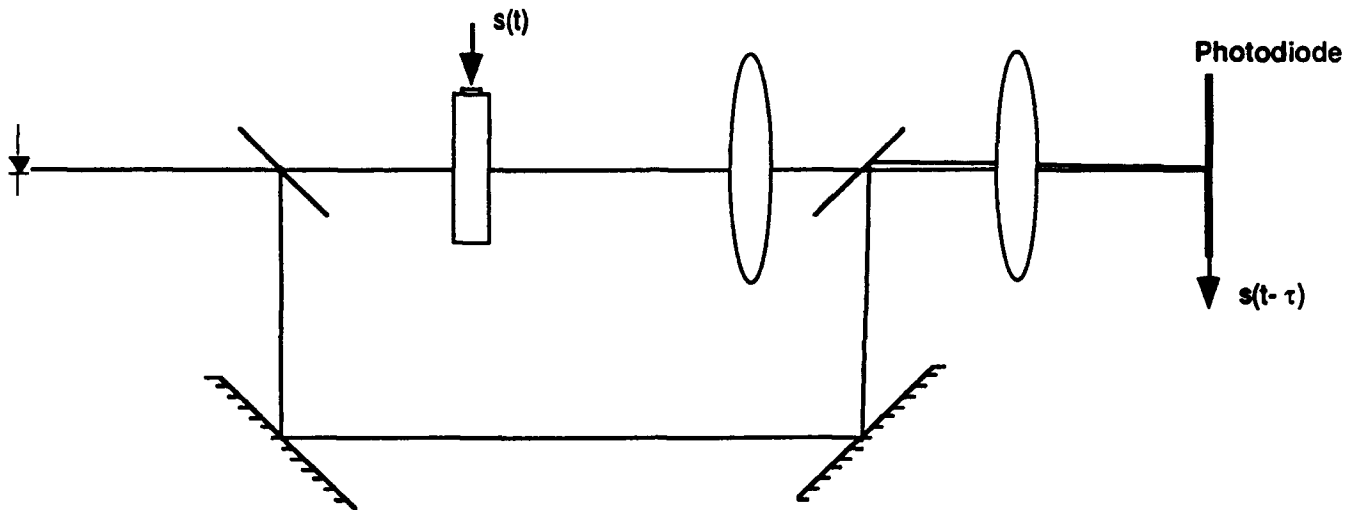


Figure 2-6. Simplified Image Plane Architecture to Delay a Signal

The signal to be delayed drives acousto-optic Bragg cell in the upper leg of the Mach-Zehnder interferometer to modulate a coherent laser beam. A pair of lenses images the signal Bragg cell onto the photodiode so that a time-delayed replica of the signal driving the Bragg cell illuminates each location of the Bragg cell with the time delay proportional to distance along the photodiode. The reference beam traveling through the lower leg of the interferometer is a focused spot on the photodiode. As shown in Figure 2-7, heterodyne detection of the steering beam spot with the signal imaged from the Bragg cell in effect taps the Bragg cell. The output signal from the photodiode is a time delayed version of the input signal driving the signal Bragg cell with the delay determined by the location of the steering beam spot on the photodiode.

The optical reference beam traveling through the lower leg of the interferometric architecture in Figure 2-6 is focused to a point on the face of the photodiode (see Figure 2-7).

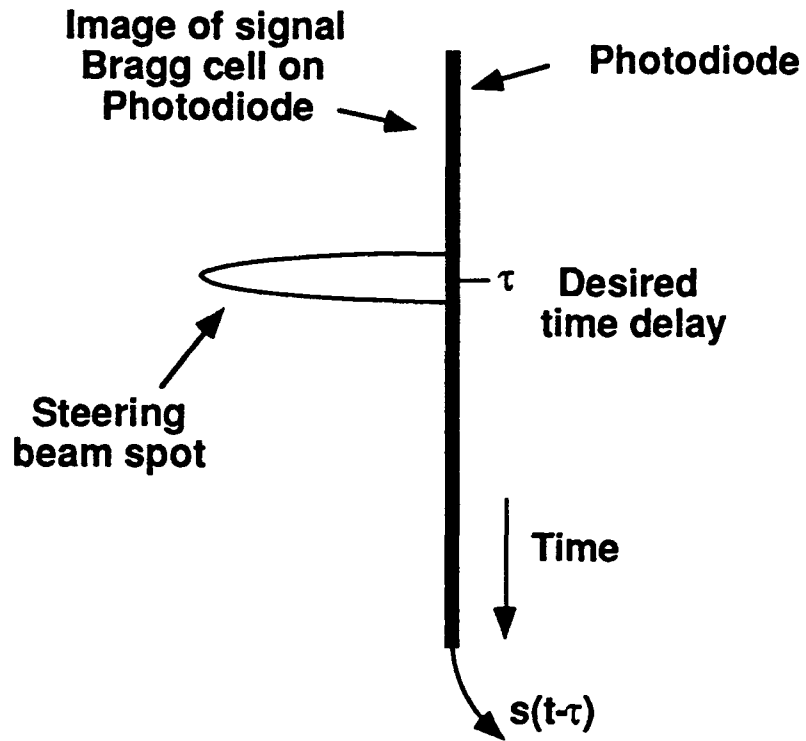


Figure 2-7. Tapping the Signal Bragg Cell on the Photodiode

Section 3

ARCHITECTURES

This section presents and defines the acousto-optic based true time delay beamforming architectures that were considered on this effort, and the operational modes of these architectures.

3.1 Processor Structures versus Operational Modes

Acousto-optic true time delay beamforming architectures were identified that are applicable for a range of configurations of RF arrays and their operational modes. These configurations/operational modes fall into the following categories:

Transmitting versus receiving arrays,

One-dimensional linear versus two-dimensional planar,

Single versus multiple simultaneous beams,

Single versus multiple signals.

Architecture refers to the structure of the processor. The two primary classes of architectures are time domain (Image Plane) and frequency domain (Fourier Plane). The principle of how these architectures generate time delays is described above in Section 2.3. In addition to the Image versus Fourier Plane categorization, there exists both a single-element and a multi-element version of both the Fourier and the Image Plane architectures. A single-element processor generates a time delayed signal for just one of the array elements of an RF array; a multi-element processor generates time delayed signals for a number of, or all of, the elements of an RF array. Single- versus multi-element processors are discussed further in Section 3.5. The single-element processor architectures can be used to steer one-dimensional curved or two-dimensional conformal arrays. The multi-element processor architectures are not well suited for use with these arrays.

As will become evident in this section, each of the architectures can be applied to each of the configuration/operational modes listed above.

3.2 Fourier Plane Architecture for Linear Transmitting Arrays

To use the acousto-optic Fourier Plane architecture to form a beam for a linear transmitting array, multiple photodiodes (one for each element of the array) are needed in the Fourier transform plane of the signal Bragg cell in order to create the multiple time delayed replicas of the signal to be transmitted. Furthermore, each of these photodiodes must be illuminated by a reference plane wave with a different angle of incidence in order to generate the set of time delays required to steer the array. When scanning the formed beam, the differences in the time delays must remain proportional to one another, with the constants of proportionality determined by the separation between the RF array elements. Movable mirrors, or multi-channel Bragg cells could be used to control the orientations of the reference plane waves and maintain the proportionality relations between the changes of time delay. The approach taken here for steering a transmitting linear array is to use a single-channel steering Bragg cell and a stack of angle amplification optics (such as prisms or pairs of lenses) to create and control the multiple plane waves illuminating the photodiodes (see Figure 3-1).

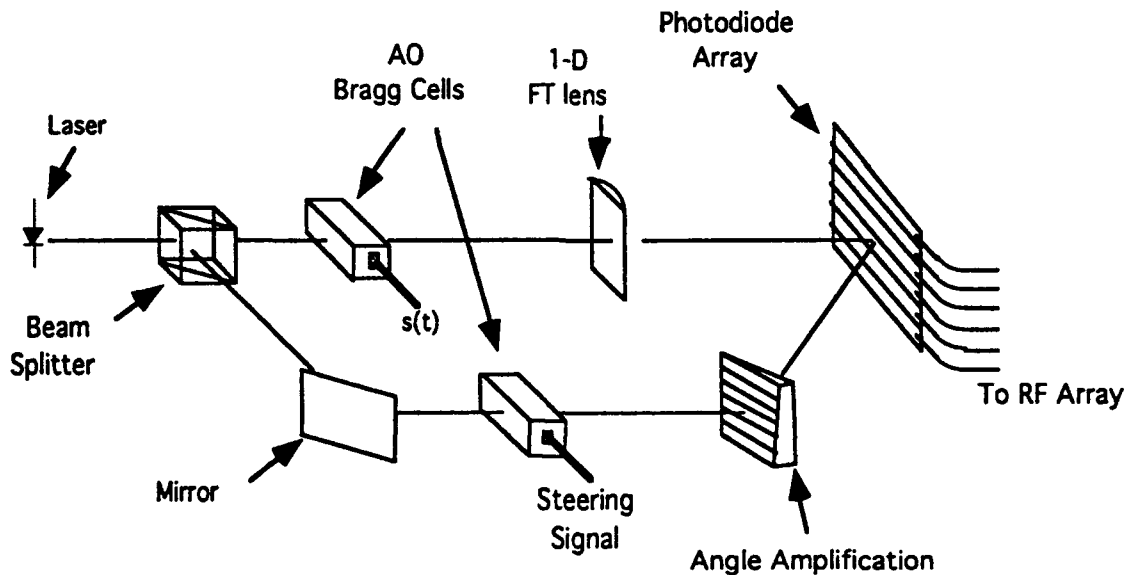


Figure 3-1. Fourier Plane Architecture for a Transmitting Linear Array

The change in angle of a reference beam on a photodiode must be some fixed factor (may be less than, equal to, or greater than unity) times the change of angle out of the steering Bragg cell as a result of change of frequency of the steering signal. That is, the amplification factor

must be fixed, but different, for each photodiode. Analysis of using prisms versus lens pairs for angle amplification is presented in Section 4.1.

The advantage of the multi-channel Bragg cell, single element delay modules, or deformable mirror approach is that they allow for flexibility in beam shaping and provide the capability to form a beam with a conformal array. The advantage of using a single-channel Bragg cell with angle amplification optics is that the array can be scanned by simply changing the frequency of a single signal which is a tone.

The acousto-optic architecture shown in Figure 3-1 for generating and controlling a set of time delays for linear transmitting arrays is now described. The signal $s(t)$ to be transmitted by the linear array drives the acousto-optic signal Bragg cell in the upper leg of the interferometer. Coherent light from the laser source passing through this Bragg cell is modulated by the signal $s(t)$. This modulated light passing through the Fourier transform lens results in the spectrum of the signal, which illuminates a column of wideband photodiodes. Ideally, each photodiode is narrow in the vertical dimension and wide in the horizontal dimension. The photodiode must be wide enough to catch the full spectrum of the signal.

The signal out of each photodiode is the detected interference between the signal spectrum and the reference plane wave, integrated over the width of the photodiode (i.e., integrated over spectral frequency). This output signal is a delayed replica of the input signal, with the delay determined by the angle between the reference plane wave and the upper leg of the interferometer as described in Section 2.3.1.

An electrical steering signal (a single frequency tone for forming and steering a single beam, multiple tones for forming and steering multiple beams) drives the steering Bragg cell in the lower leg, the beam steering leg, of the interferometer. The purpose of the angle amplification optics in the steering leg is to map the single beam out of the steering Bragg cell into multiple plane waves having a range of orientations necessary to generate the desired range of time delays. Optics not shown in the beam steering leg are necessary so that each of these reference plane waves illuminates the corresponding photodiode. The result is that the orientations of the reference plane waves on the photodiodes, and therefore the set of time delays, is controlled by the frequency of the single steering signal and by the angle amplification optics in the beam steering leg.

The control signal in the steering Bragg cell results in a frequency shift of the optic reference beam by an amount equal to the frequency of the steering signal. The frequency shifted reference beam then frequency shifts the electrical signals out of the photodiodes. If this frequency shift is not acceptable and a single-toned steering signal is being used to form a single beam, then this Doppler shift can be compensated for by either adjusting the IF of the signal driving the signal Bragg cell by an amount equal to the Doppler shift or by placing an acousto-optic point modulator in the reference leg before the beam steering Bragg cell and use it to shift the frequency of the reference beam in the opposite direction of the frequency shift imparted by the steering Bragg cell. In the case that a multi-channel steering Bragg cell is used to control the RF beam scanning, the frequency shift imparted by the the control signals must be removed since in this case the signal emitted by each array element is frequency shifted by a different amount. This is destructive to the signal formed by the array. For the multi-channel steering Bragg cell case, the necessary frequency compensation can be achieved with a multi-channel point modulator placed before the steering Bragg cell in the reference leg of the processor.

3.3 Architectures for Linear Receiving Arrays

Figure 3-2 shows a Fourier Plane architecture to achieve true time delay beamforming for a one-dimensional (linear) receiving array. In order to form a beam in a particular direction with a receiving linear RF array, the outputs of the array elements must be delayed relative to one another and then summed. The amount of relative delay between array elements is determined by the spacing between the array elements and by the angle between the beam and the normal to the array.

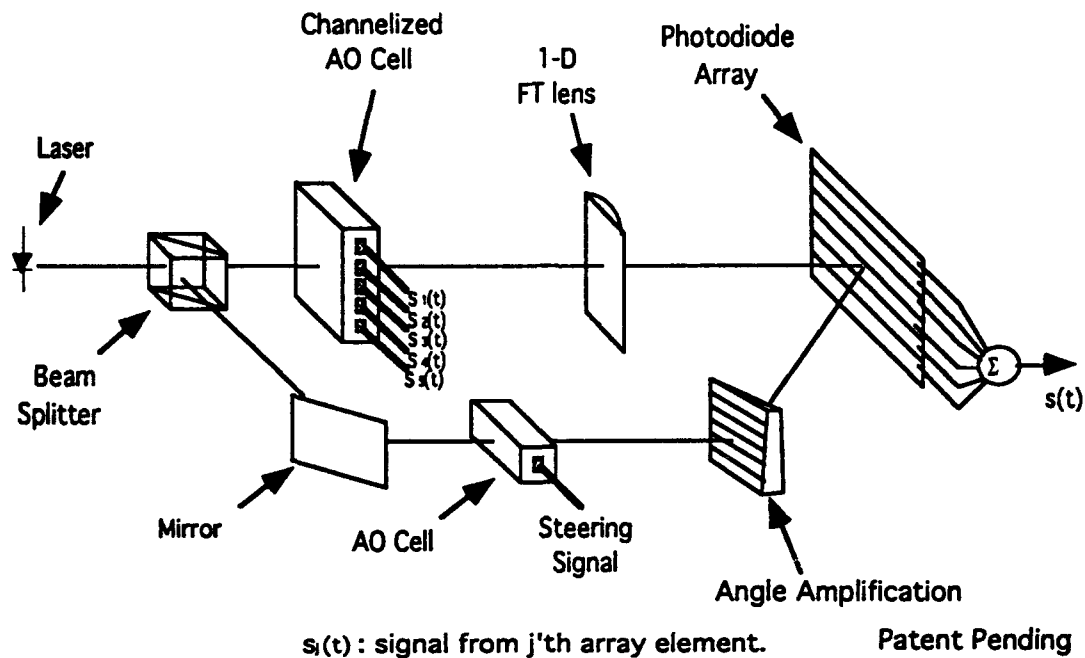


Figure 3-2. Fourier Plane Architecture of a Receiving Linear Array

The principle of how the Fourier Plane architecture shown in Figure 3-2 for a receiving array delays a signal is the same as for the Fourier Plane architecture for the one-dimensional transmitting array shown in Figure 3-1 and described in Section 3.2. In the case of a receiving array, a multi-channel Bragg cell is used in the upper leg of the interferometer in Figure 3-2, with the number of channels equal to the number of antenna elements in the linear array, or equal to the number of subarrays. Here, an electrical signal from each element of the receiving array drives a channel of the multi-channel Bragg cell. The signal in each channel is optically Fourier transformed onto a corresponding photodiode in the array of photodiodes. As described in Section 2.3.1, the electrical output of a photodiode is a time delayed replica of the electrical signal that drives the corresponding channel of the multi-channel Bragg cell. The time delay is determined by the angle between the reference plane wave from the lower leg of the interferometer and the face of the photodiode.

The steering leg of the interferometer, the lower leg of the interferometer in Figure 3-2, functions identically to the steering leg in the transmitting architecture shown in Figure 3-1. The angle amplification optics in the steering leg results in reference plane waves having a distribution of angles incident on the array of photodiodes. This allows a single-channel Bragg cell, driven with a tone, to control a range of time delays.

The electrical outputs of the photodiodes are summed together to generate the desired signal. This sum forms a replica of the signal arriving at the linear antenna array from the direction determined by the frequency of the steering signal.

3.4 Multiple Beam Capabilities

A single beam is formed, corresponding to one delay out of each photodiode, when the steering signal is a single tone. In the case that the steering signal is a sum of tones, the signal out of each photodiode is a sum of time delayed replicas of the signal driving the signal Bragg cell, and multiple simultaneous beams are formed. The number of simultaneous beams is equal to the number of tones in the steering signal. Each of these beams can be formed independently.

For the transmitting case the same signal is transmitted on each of the beams. Each of these beams is Doppler shifted by a different amount equal to the steering signal frequency for that beam. This different Doppler shift on each beam, is up to on the order of 5 MHz for transmitting a wideband signal (e.g., 1 GHz). This Doppler shift cannot be easily removed for the case of multiple simultaneous beams.

For the case of receiving simultaneous multiple beams, the resulting signal is the sum of the signals received by the multiple beams. If a number of signals, each at a different location, are to be received, and each of these signals is in a different frequency band, then these signals can be obtained simultaneously by passing the sum signal through the appropriate bank of band pass filters.

3.5 Single- versus Multi-Element Modules and Single- versus Multiple-Signals

Single-Element Modules

The Fourier Plane and Image Plane architectures as described above are multi-element module architectures. That is, each module generates time delays for a number of antenna array elements. A single-element module generates a time delayed signal for a single element of the RF array. Therefore, for the single-element module case there must be one single-element module for each array element, or subarray, of the RF array. An Image Plane architecture version of a single-element module is shown in Figure 3-3. Each single-element module is much simpler than a multiple-element module, and they can be identical. The range of time

delays are generated by using a different steering signal frequency to drive the steering Bragg cell in each module rather than using different angle amplification for each delay. The structure is one-dimensional and may be a good candidate for implementation in integrated optics.

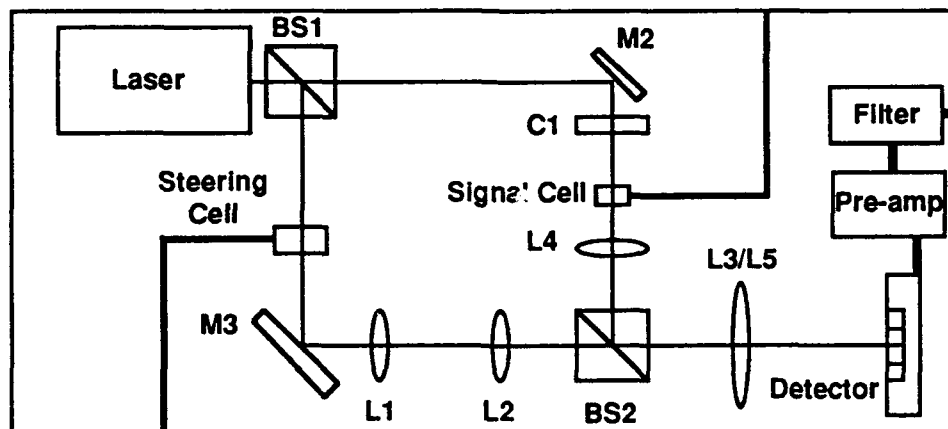


Figure 3-3. Image Plane Version of a Single-Element Module Architecture

The disadvantages of using a number of single-element modules as opposed to using a single multi-element module are the need to generate and control multiple steering signals, one for each single-element module; the need to compensate for the Doppler shift imported by the steering signal Bragg cell in each of the single-element delay modules; and most seriously, the difficulty of controlling the phase differences between the delayed signals out of the different single-element modules. This issue of controlling the phases of the time delayed signals at the RF carrier frequency is addressed in detail in Section 4.2.

Multiple Signals

Simultaneously transmitting or receiving more than one signal with the array requires that one time delay module be used per signal per element of the RF array. Figures 3-4 to 3-7 show how multi- and single-element modules can be used to transmit and receive single and multiple signals simultaneously. Note that a single-element time delay module generates a time-delayed signal for a single element of the antenna array. The number of single-element modules required is equal to the product of the number of antenna array elements times the number of signals to be transmitted simultaneously.

A multi-element time delay module generates time delays for a number of array elements. The number of multi-element delay modules that provide signals to an RF array element is equal to the number of signals to be transmitted simultaneously.

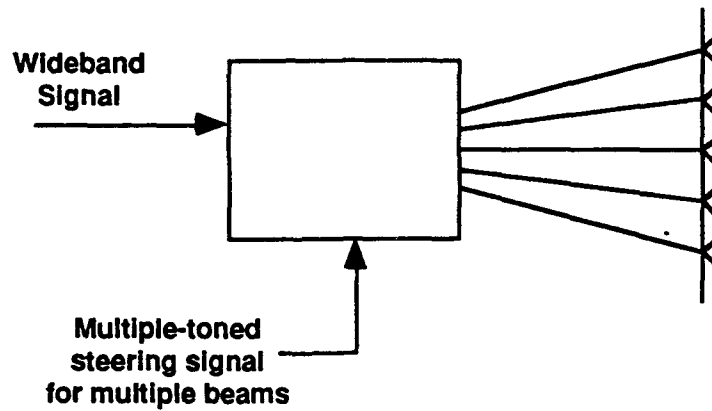


Figure 3-4. Transmitting Multiple Signals Using One Multi-Element Module

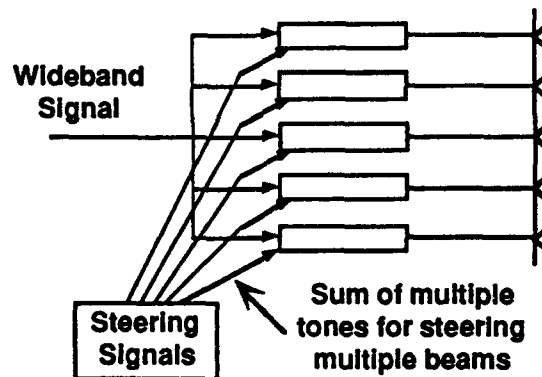


Figure 3-5. Transmitting a Single Signal Using Single-Element Modules

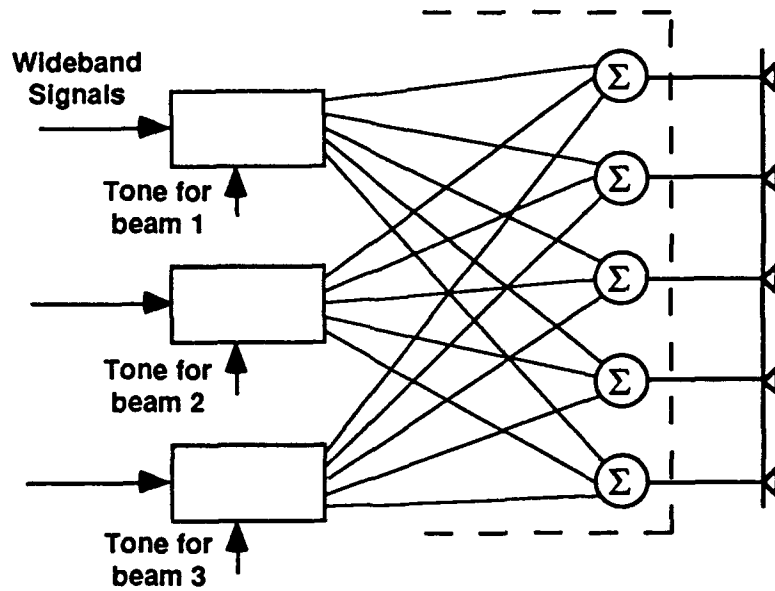


Figure 3-6. Transmitting Multiple Signals Using a Multi-Element Module for Each Signal

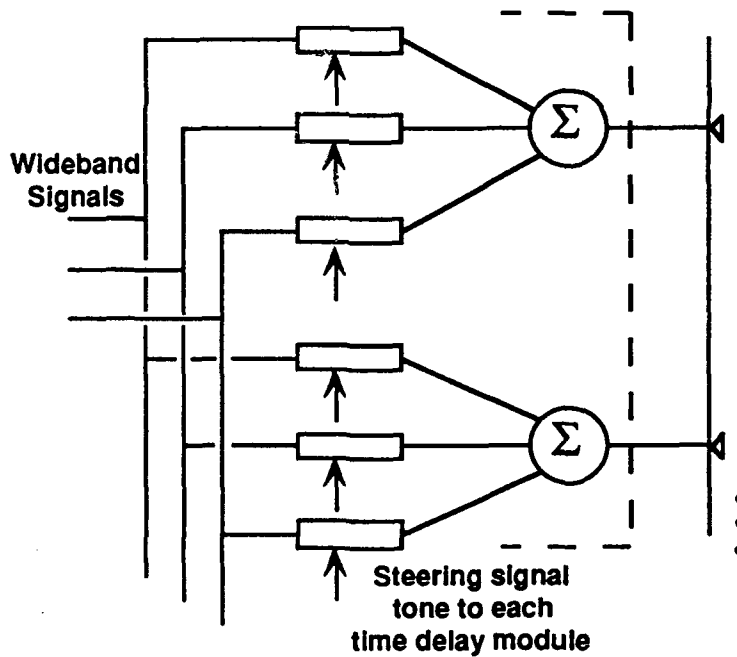


Figure 3-7. Transmitting Multiple Signals Using a Single-Element Modules

3.6 Planar Arrays

True time delay architectures for linear arrays can be used for planar arrays. The key is that the elements of the planar array that lie on the same line normal to the projection of the RF beam pointing direction onto the face of the array all receive the same time delay (see Figure 3-8). In order to use the linear array true time delay architectures for planar arrays, a switching network is needed to route the time delays to the appropriate planar array elements. The azimuth of the beam is determined by which elements are excited by the same time delay. Beam elevation is determined by the time delays. Additional phase shifts need to be applied to the array elements that do not lie on one of the lines corresponding to a generated time delay.

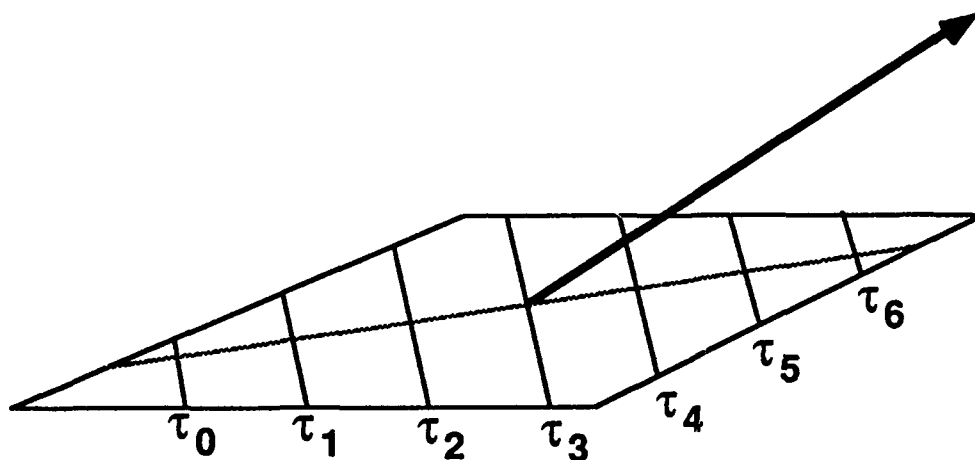


Figure 3-8. Mapping of Set of Time Delays to a Planar Array

Section 4

ANALYSIS OF TECHNICAL ISSUES

In this section several, key technical issues are identified and addressed. These are issues that need to be considered before a preliminary design is developed. The issues considered here are implementation trades of the angle amplification of the optical steering beam; the need and means for providing phase shifts to the carrier so that the phases of the carrier will be correct at the operating RF of the array; photodiode considerations; and the generation of sidelobes due to spurious time delays and how to control the level of these sidelobes. Further analysis of the photodetector in terms of SNR are reported in Section 5.

4.1 Angle Amplification

Amplification of the diffraction angle of the optical beam out of the steering Bragg cell is required with a range of amplifications. The angle amplifications required are proportional to the relative position of the elements of the RF array. With a range of angle amplifications, a single tone driving the steering Bragg cell results in optical beams having a range of orientations and the generation of a set of signals with the necessary delays to form a beam.

Two methods for implementing optical angle amplification were considered: 1) with prisms, and 2) with lens pairs.

4.1.1 With Prisms

The change of angle of an optical beam out of a prism compared to the change of angle out of the steering Bragg cell depends on the wedge angle α of the prism and the orientation of the prism relative to the Bragg cell. Thus, it is possible that a stack of prisms with different wedge angles and orientations might allow a single channel Bragg cell to be used to steer the array, provided that the required proportionality relations between the changes in the relative time delays can be maintained. Figure 4-1 depicts the angles for describing the use of a Bragg cell and prisms to generate and control the set of reference plane waves.

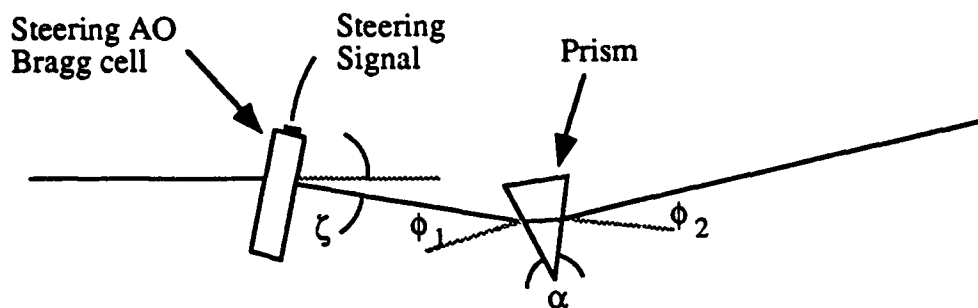


Figure 4-1. Angles for Describing Bragg Cell/Prism Optical Beam Control

The angles shown in Figure 4-1 are defined as follows:

- ζ = angle of deflection out of the Bragg cell,
- ϕ_1 = angle of incidence of the deflected optical beam on the input face of the prism, measured from the face normal,
- δ = orientation angle of the prism measured between the normal to the input face of the prism and the undeflected optical reference beam,
- α = wedge angle of the prism,
- ϕ_2 = angle between the reference beam out of the prism and the normal to the output face.

The deflection angle out of the the steering Bragg cell is given by

$$\zeta = 2 \cdot \arcsin \left[\frac{\lambda}{v_a} \cdot f \right], \quad (4.1)$$

where,

- λ = wavelength of the optical reference beam,
- v_a = acoustic velocity in the Bragg cell,
- f = frequency of the electrical signal driving the steering Bragg cell.

The angle of incidence of the deflected plane wave on the input face of the prism is

$$\phi_1 = \zeta + \delta. \quad (4.2)$$

The orientation of the optical beam out of the prism, measured from the normal to the output face, is

$$\phi_2 = \arcsin \left[\frac{n_2}{n_1} \cdot \sin \left[- \arcsin \left[\frac{n_1}{n_2} \cdot \sin (\phi_1) \right] + \alpha \right] \right] \quad (4.3)$$

where,

n_1 = index of refraction of air,

n_2 = index of refraction of the prism.

Figure 4-2 contains plots of the angle out of the prism versus the input angle for 5 different prism wedge angles. Figure 4-3 is a plot of the angle amplification of the prism versus input angle for the same 5 prism wedge angles. The angle amplification is defined as the rate of change of output angle to change in input angle.

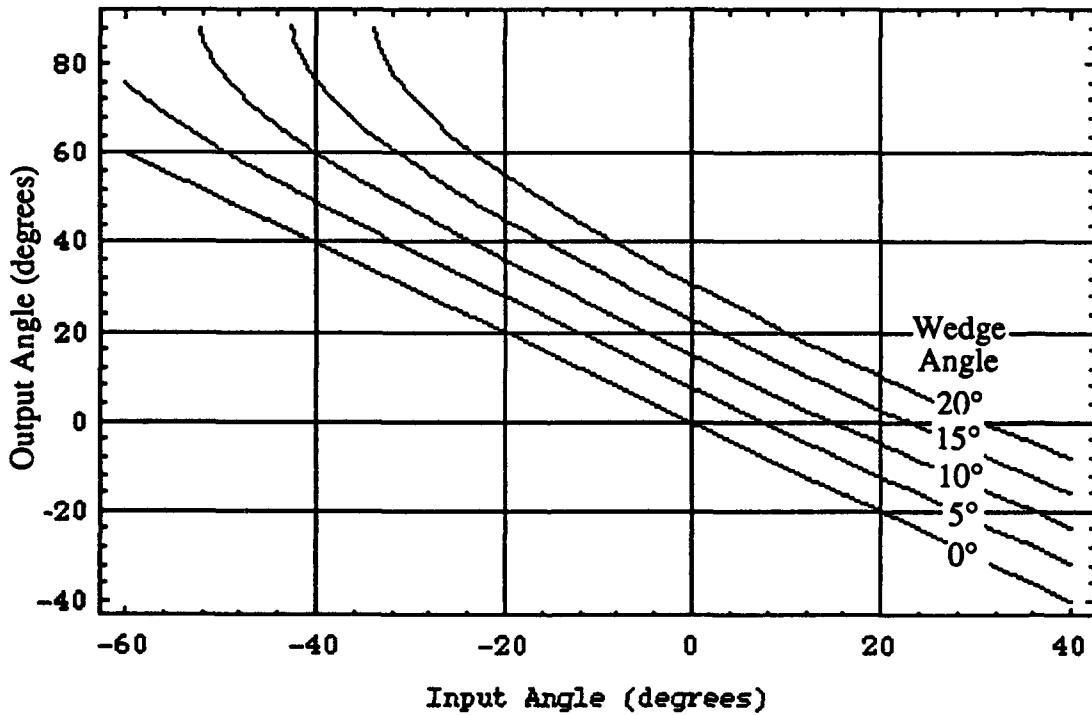


Figure 4-2. Output Angle from Prism versus Input Angle for Five Different Prisms Wedge Angles

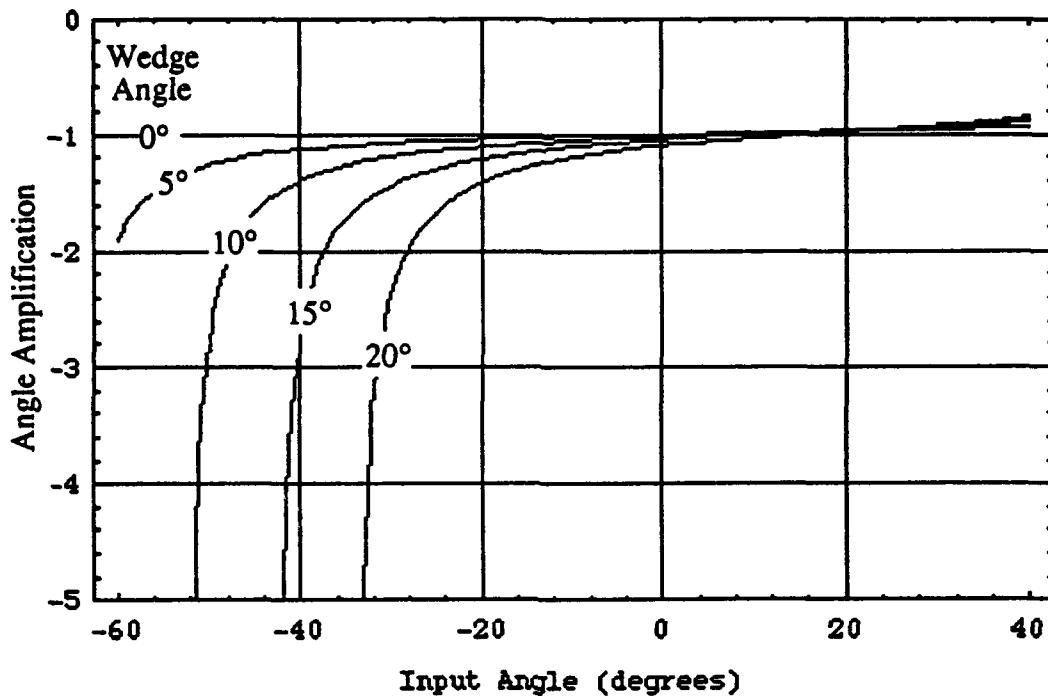


Figure 4-3. Angle Amplification Input Angle for Five Different Prism Wedge Angles

Note that the angle amplifications are not large except when they become highly nonlinear with respect to input angle. The nonlinearity will result in broadening of the beam formed by the RF array as it is steered away from the normal to the array when trying to use a signal with a single tone to steer the array.

4.1.2 With Lenses

The use of convex lens pairs (see Figure 4-4) is far superior to that of using prisms. The configuration shown in Figure 4-4 is a 2-F imaging system.

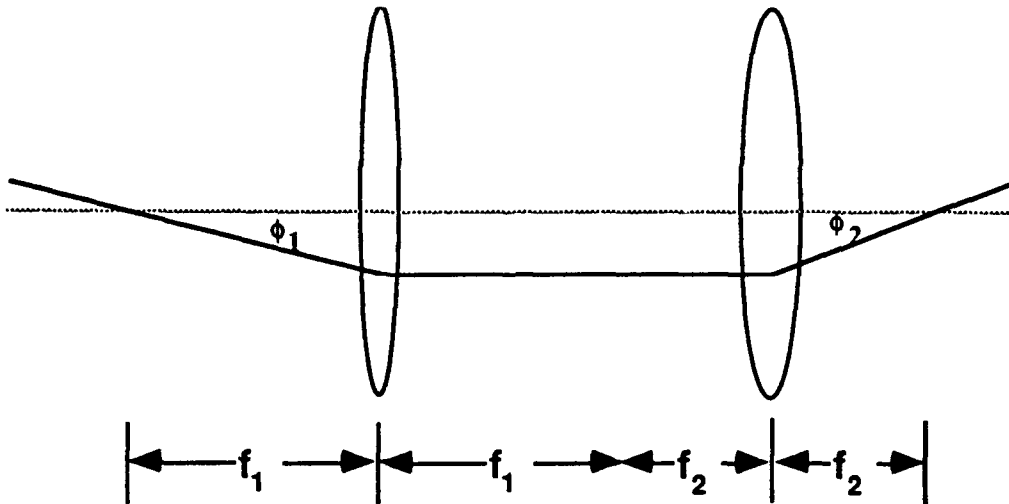


Figure 4-4. Pair of Concave Lens for Angle Amplification

Angle amplification is defined as the derivative of the output angle with respect to the input angle:

$$A = \frac{d\phi_2}{d\phi_1} . \quad (4.4)$$

In terms of the focal lengths and the input angle, the angle amplification is given by

$$A = \frac{f_1}{f_2} \frac{1}{\cos^2(\phi_1) + \frac{f_1}{f_2} \sin^2(\phi_1)} . \quad (4.5)$$

For small input angles, the amplification is approximately independent of input angle and is, to a good approximation, the ratio of the focal length of the first lens to that of the second lens

$$A \cong \frac{f_1}{f_2} . \quad (4.6)$$

Thus, the required proportionality between the angle amplifications of the optical steering beams can be maintained over the full range of scan angles of the RF array.

4.1.3 Recommendation

The recommendation is to use lenses for angle amplification. Angle amplification with lenses is nearly independent of input angle, whereas it depends on input angle in a nonlinear way for prisms.

4.2 Carrier Phase Adjustment for IF to RF Translation

Not only must the envelope of the wideband signal be properly delayed from one array element to the next, but the phase of the RF carrier must also be properly delayed in order to form a beam in the desired direction.

The acousto-optic Fourier Plane and Image Plane time delay architectures described in Section 3 correctly delay the modulation envelope of the signal as well as correctly phase shift the carrier at the IF at which the signal is delayed. An additional phase shift is required on the carrier when translating to the RF of the array. This additional phase shift for a delay τ is given by

$$\Delta\phi = 2\pi \cdot \tau \cdot (\text{RF} - \text{IF}) . \quad (4.7)$$

This phase shift correction can be implemented by placing a transparent wedge in a Fourier plane of the steering Bragg cell of the time delay generator, as shown in Figure 4-5. The taper and orientation of the wedge and its index of refraction determine the phase shift adjustment as a function of time delay.

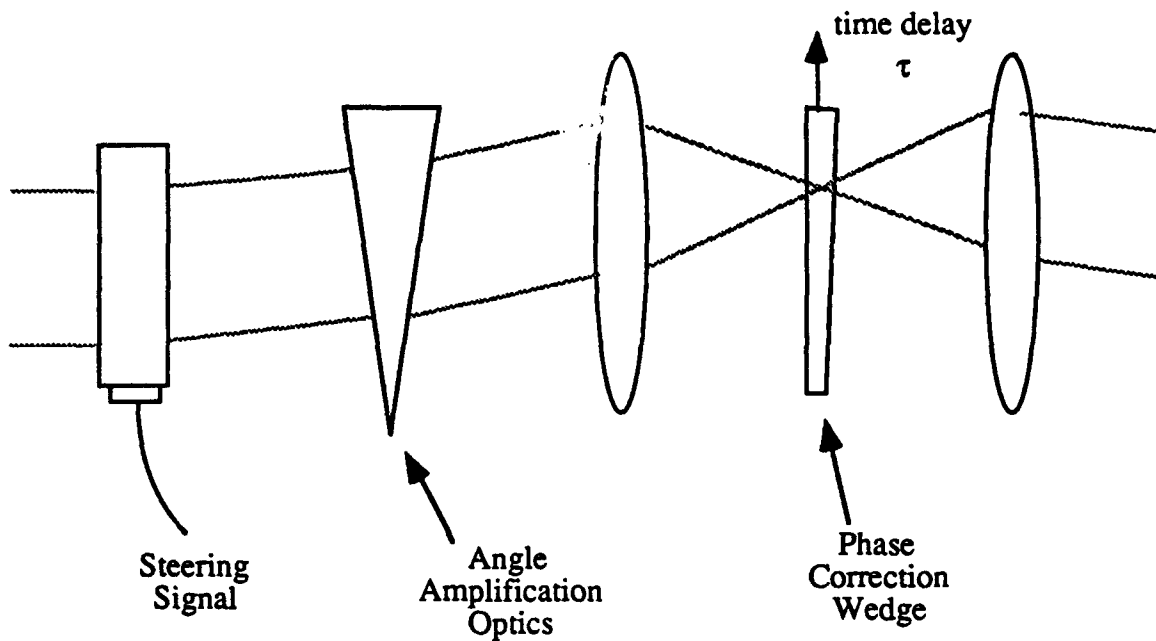


Figure 4-5. Use of Wedge to Provide Time Delay Dependent Phase Adjustment

The reason the use of the wedge works to provide the required phase shift given by Equation (4.7) is that the steering beam focuses to a point in any Fourier plane of the steering Bragg cell. The lateral distance along the wedge to this point is proportional to the time delay that will result. The phase shift in the steering beam, as a result of passing through the wedge, is

$$\Delta\phi = x \cdot (n - 1) \quad (4.8)$$

where x is the thickness of the wedge at the position at which the steering beam passes and n is the index of refraction of the wedge material. Since x is proportional to the desired time delay, and the phase shift correction is to be proportional to the time delay, the thickness of the wedge must change proportionally to the lateral distance along the wedge.

The requirements on the tolerances of the wedge are addressed in Section 5.3.3.

4.3 Photodiode Considerations

The first fundamental constraint on the photodiode array is that the number of photodiodes in the array must be equal to the number of array elements to be fed per time delay module. The second constraint is that the bandwidth of each photodiode in the array must be equal to the IF of the processor plus one-half the signal bandwidth.

An additional critical requirement on the photodiode is that the detector noise be sufficiently low relative to the signal in order to provide a system signal-to-noise ratio in excess of 30 dB.

For the Image Plane architecture the width of the photodiode must be equal to the width of the magnified image of the signal Bragg cell, and, in general, can be narrower for higher bandwidths. This is consistent with the dependence of photodetector bandwidth on size. For the Image Plane architecture, the photodiode can be segmented and those segments containing the desired delays can be output. This reduces noise contributions from shot noise and dark current if these noise contributions are significant compared to other detector noise contributions.

For the Fourier Plane architecture the width of the photodiode is equal to the width of the signal spectrum in the Fourier plane. The higher the bandwidth of the signal the wider the photodiodes must be. On the other hand, higher bandwidth photodiodes are by necessity smaller (within a given detector technology).

The photodiode considerations favor the Image Plane architecture, particularly for use with wideband signals.

4.4 RF Array Sidelobes

It is important that the sidelobes of an RF array be low. The factors that determine the positions and amplitudes of the beam sidelobes are array element positions and weights. Additionally, spurious time delays may result in sidelobes. How spurious time delays might occur can most clearly be seen by considering the Image Plane architecture. Spurious time delays result from the sidelobes of the optical reference (steering) beam on the detector. Figure 4-6 depicts the optical reference beam, and including its sidelobes, on the detector.

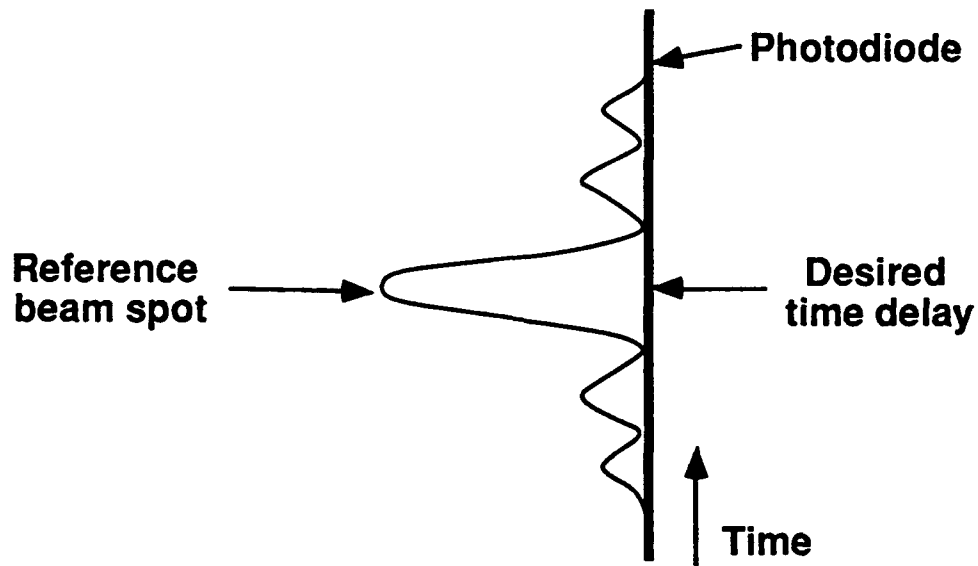


Figure 4-6. Reference Beams with its Sidelobes on the Photodiode

How the spurious time delays from the different detectors line up determines whether they generate an RF beam sidelobe, echoes in the desired beam, or noise. For uniformly spaced RF array elements, the angle of the line connecting reference beam spots on the detector array, main and sidelobes, determines the pointing directions of the RF array main beam and sidelobes. If the lines connecting the optical sidelobes on the photodiode array (see Figure 4-7) have different slopes than the line connecting the main lobe of the reference beam, then the spurious sidelobes will result in RF array beam sidelobes.

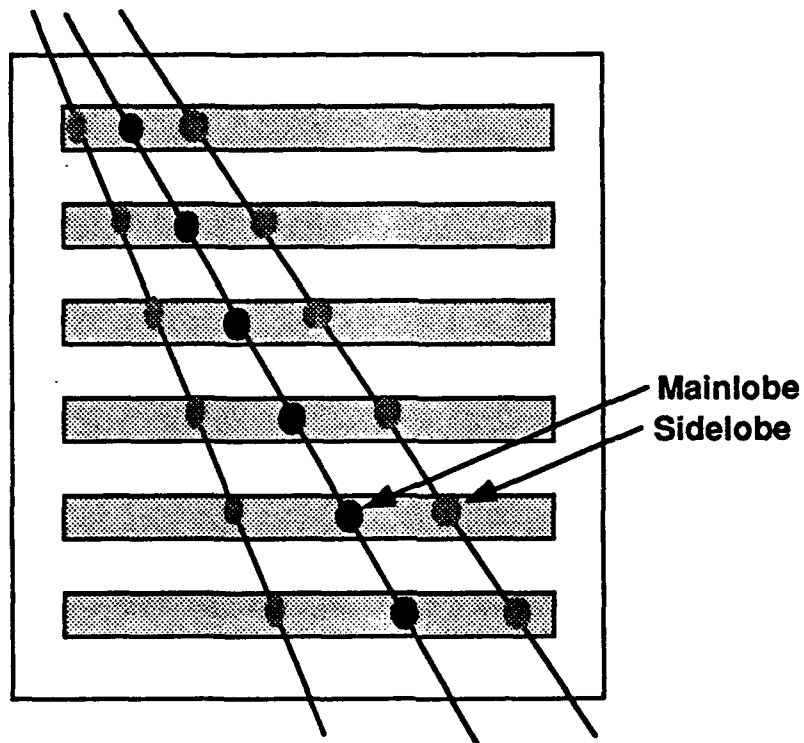


Figure 4-7. Generation of RF Array Sidelobes from the Spurious Time Delays

If the lines connecting the reference beam sidelobes on the photodiode array have the same slope as the line connecting the main lobes (see Figure 4-8) then echoes (pre and post) will be generated by the array.

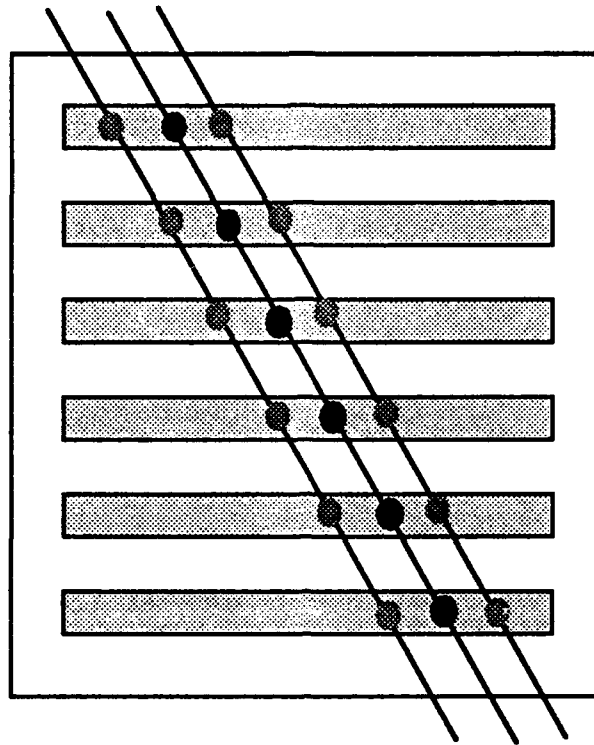


Figure 4-8. Generation of Echoes from the Spurious Time Delays

Analysis shows that RF sidelobes, not echoes, are created by the proposed architectures. The optical sidelobes are a result of the steering Bragg cell aperture. Magnifications in the steering arm are proportional to antenna element location. Optical reference null and sidelobe locations scale with the magnification. Therefore, the lines connecting sidelobes peaks diverge linearly with time delay, resulting in the generation of RF sidelobes.

In order to maximize the energy in the main beam of the RF array and minimize noise contributions, it is important to minimize, within reason, the sidelobes of the optical steering beam.

The sidelobe structure and levels of the optical steering beam at the detector are determined by how the optical beam is apertured, and by the profile of the beam at the aperture. The profile of the optical beam is Gaussian truncated by the aperture of the steering Bragg cell. The sidelobe levels can be controlled by what fraction of the Gaussian passes through the aperture. The farther out in the tails of the Gaussian is truncated, the lower the sidelobes, but the larger the steering beam spot on the detector (for the image plane architecture).

The sidelobe level of the optical steering beam must be traded against spot size on the photodiode by varying the truncation ratio of the Gaussian. The trades are:

To minimize the sidelobe level,

To obtain a small enough spot to avoid low-pass filtering of the signal. The spot must be no wider than the reciprocal of the signal bandwidth.

Optical system component parameters determine maximum spot size permitted. The velocity of sound in the signal Bragg cell and the focal lengths of the lenses that image the signal Bragg cell onto the detector determine the dimension on the detector that corresponds to the reciprocal of the bandwidth of the signal.

Figure 4-9 depicts the trade between sidelobe level and spot size of the optical beam. This figure is a plot of normalized spot size versus sidelobe level. A normalized spot size of 1 corresponds to the spot size that would occur for an optical beam that is uniform at the aperture, that is the amplitude of the beam does not vary across the aperture.

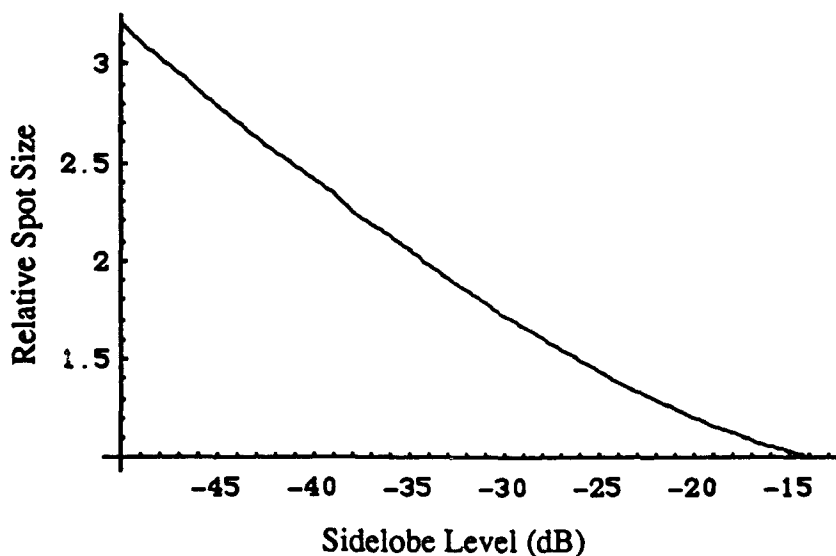


Figure 4-9. Relative Spot Size of Steering Beam versus Sidelobe Level

Figure 4-10 shows the relationship between sidelobe level and truncation ratio of the Gaussian beam. A truncation ratio of 1 corresponds to truncating the Gaussian at the $1/e$ level.

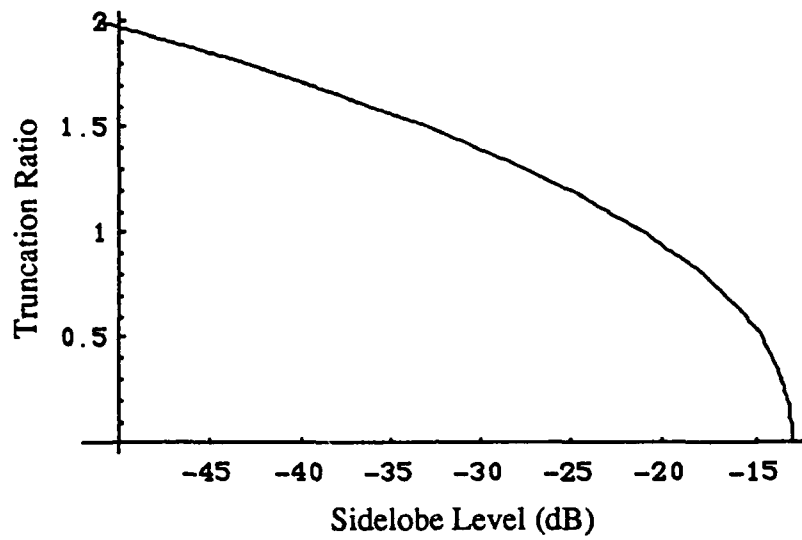


Figure 4-10. Truncation Ratio (in Units of $1/e$ Points) as a Function of Desired Sidelobe Level

From Figure 4-9, a good choice for relative spot size is 2 which provides a sidelobe level of -35 dB. From Figure 4-10 this sidelobe level is obtained when the Gaussian truncation ratio is about 1.6.

Section 5

DEMONSTRATION BREADBOARD

In this section the key design concerns for the proof-of-principle demonstration breadboard are presented. The emphasis here is to present the parametric relationships that drive the selection of the values of the design parameters. The methodology presented here can be used develop the designs in follow-on phases of the development of the acousto-optic true time delay beamformer. Even though the breadboard design is based on the Image Plane architecture, the methodology presented here is also applicable to the development of a time delay generator based on the Fourier Plane architecture.

The key design topics addressed here are the selection of the lens focal lengths and Bragg cell parameters, design parameters of the phase correction wedge, and the performance issues of optical efficiency and SNR, and sensitivity of scan angle to the frequency of the steering signal.

5.1 Strawman Requirements and Constraints

It is desired that the proof-of-principle breadboard be able to demonstrate the ability to generate and control time delays that would be required to steer an array over a wide field-of-view when transmitting (receiving) a wideband signal. The following strawman requirements are selected for this demonstration:

Signal bandwidth	1 GHz
Transmitted RF	10 GHz
Maximum steering angle	$\pm 60^\circ$
Array length	2 m

The development and demonstration of the proof-of-principle unit is constrained by a limited budget. Therefore, the constraints on the design of the demonstration unit are that it be low cost, and that it be implementable with commercial lenses to avoid the expense of custom lens design and fabrication. A primary risk and budget driver is the high signal bandwidth of 1 GHz at which the unit will be demonstrated. The high bandwidth pushes up the cost of the signal Bragg cell, photodetector, and signal generation and test equipment. Furthermore, the

signal-to-noise performance for a given optical power decreases as bandwidth increases. Never the less there is a great benefit to be gained in demonstrating the unit at the kind of bandwidths for which such a system would be needed. It is felt that the demonstration breadboard as designed can be built and can demonstrate, within budget, proof-of-principle performance at the 1 GHz signal bandwidth.

5.2 Breadboard Architecture Selection

The Image Plane architecture is used as the basis for the design of the breadboard demonstration unit. The Image Plane architecture provides greater flexibility in lens selection than the Fourier Plane architecture, and the required photodiode sizes are better matched for the demonstration bandwidth and IF.

5.3 Breadboard Design

In this section, values for key design parameters for the breadboard are established. The Image Plane architecture for a transmitting linear array is assumed. The optical layout for the demonstration breadboard is shown in Figure 5-1. The key parameters considered here are the bandwidths and apertures of the Bragg cells and the focal lengths of the most significant lenses: those that image the signal Bragg cell onto the photodiode, those that provide the angle amplification of the steering beam, and those that determine the relative magnification of the reference steering beam spot and of the signal Bragg cell image on the photodiode.

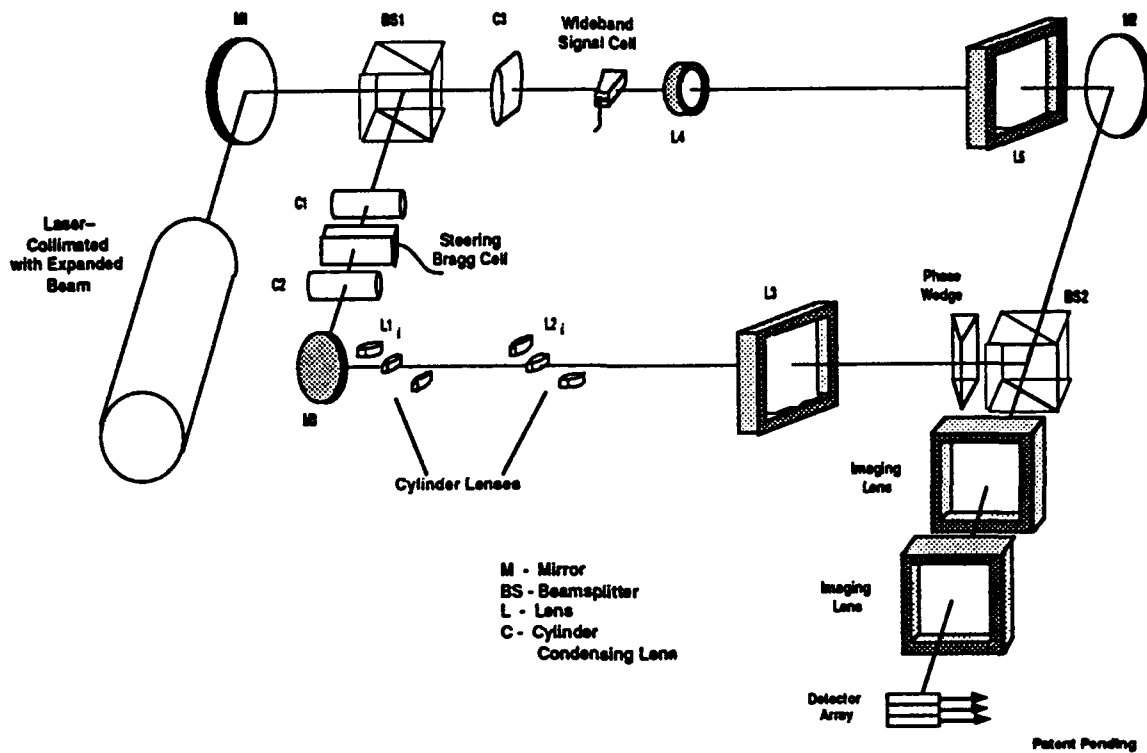


Figure 5-1. Optical Layout for the Demonstration Breadboard

5.3.1 Parametric Relationships for Selecting Lens and Bragg Cell Parameters

In this section, the relationships between the design parameters are presented. The driving requirements are that the range of time delays be sufficient to scan the array over the specified range of scan angles and the ability to handle the signal bandwidth. The parameters of concern are those of the Bragg cells and key lenses that follow the Bragg cells.

Wideband Signal Bragg Cell Requirements

The time aperture of the wideband signal Bragg cell must be equal to the range of time delays required to scan the RF array over the specified range of angles. This range of time delays is given analytically by

$$T_{\text{signal}} = 2 \frac{b \sin(\alpha_{\text{max}})}{c} \quad (5.1)$$

where

- T_{signal} = range of time delays,
- = time aperture of the signal Bragg cell,
- b = RF array length,
- α_{max} = maximum scan angle measured from the normal to the array,
- c = the velocity of light.

The factor 2 in the expression for the time aperture of the signal Bragg cell accounts for the fact that the array is scanned to either side of the normal to the array.

The physical length of the aperture of the wideband signal Bragg cell is given by

$$L_{\text{signal}} = T_{\text{signal}} \cdot v_{a_w} \quad (5.2)$$

where

- v_{a_w} = the acoustic velocity in the signal wideband Bragg cell.

Narrowband Steering Bragg Cell Requirements

The primary parameters of the steering Bragg cell are its aperture and bandwidth. The bandwidth of the steering Bragg cell is the frequency range of the steering signal that is required to steer the RF array beam over the desired range of angles. The aperture of the Bragg cell together with the focal lengths of the lenses following the Bragg cell determines the spot sizes of the steering reference beam on the photodiodes. The spot size must be less than or equal to $1/(\text{signal bandwidth})$ in terms of time scale of the signal Bragg cell image on the photodiode. If the spot size is larger than this limit, then the time delayed signal will be a bandlimited version of the signal driving the wideband signal Bragg cell. The effects of the lenses in the system (magnifications, angle amplifications) are included in the relationships below for the bandwidth and aperture of the steering Bragg cell.

The key lenses in the steering leg of the time delay generator, from the steering Bragg cell to the photodiode, are shown in Figure 5-2. In this figure lenses L1 and L2 provide the angle amplification of the steering beam, and lens L3 focuses this steering beam to a spot in an image plane of the photodiodes. Not included in Figure 5-2 is the optical wedge to implement the

scan angle dependent phase correction required for translating from IF to RF (see Section 4.2 for a discussion of the phase correction.) Only a single pair of the lenses L1 and L2 are shown in Figure 5-2. The number of pairs of lenses L1 and L2, physically placed above one another, is equal to the number of simultaneous delays to be generated, i.e., equal to the number of array elements in the linear RF array.

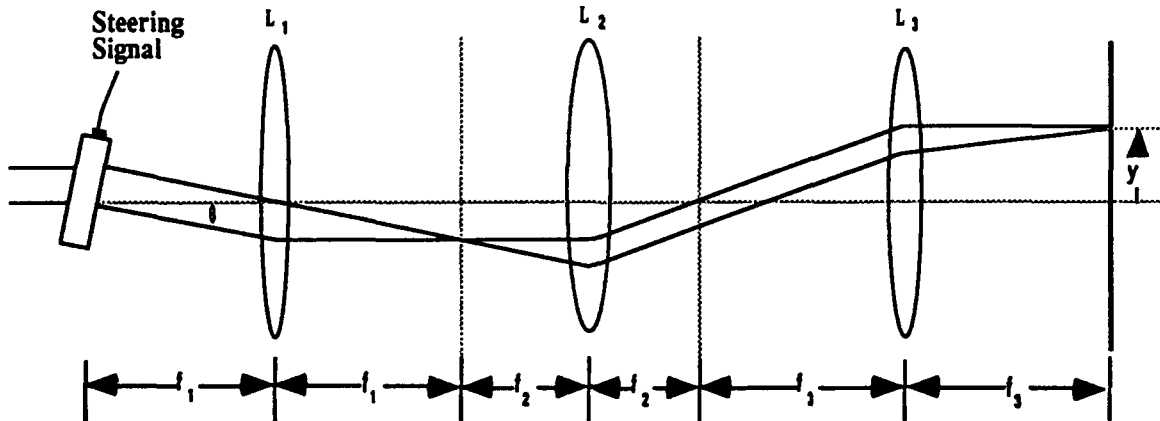


Figure 5-2. Steering Leg of the Time Delay Processor

The position of the reference steering beam spot on a photodiode is

$$y = \tan(\theta) \frac{F_1}{F_2} F_3 \quad (5.3)$$

where

- θ = the angle of the reference beam out of the steering Bragg cell measured from the optical axis of lenses L1, L2, and L3,
- F_k = focal length of the kth lens in the steering leg of the interferometer as shown in Figure 5-2.

Figure 5-3 shows schematically the signal leg of the time delay processor. The lenses L4 and L5 image the wideband signal Bragg cell onto an image plane of the photodiode with magnification determined by the ratio of focal length of lens L5 to that of lens L4.

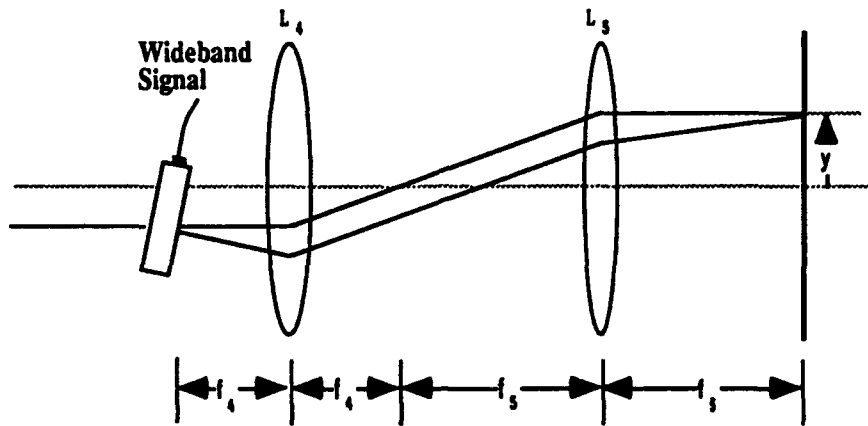


Figure 5-3. Signal Leg of the Time Delay Processor

The position along the photodiode is related to the delay time of the wideband signal:

$$y = \tau v_{a_w} \frac{F_5}{F_4} \quad (5.4)$$

where

- τ = time delay along the wideband signal Bragg cell,
- v_{a_w} = acoustic velocity of the wideband Bragg cell,
- F_k = focal length of the kth lens shown in Figure 5-2.

Combining Equations (5.3) and (5.4) to eliminate y , the following expression is obtained for the required deflection angle out of the steering Bragg cell to obtain a time delay τ :

$$\theta = a \tan \left(\frac{F_2}{F_1} \frac{1}{F_3} \frac{F_5}{F_4} \tau v_{a_w} \right). \quad (5.5)$$

To determine the steering frequency required to scan the array by an angle α from the array normal, first note that the time delay required to scan the array by an angle α is

$$\tau = \frac{b \sin(\alpha)}{c}. \quad (5.6)$$

The angle of deflection of the collimated beam out of the steering Bragg cell, as a function of the frequency of the steering signal, is given by

$$\theta = 2 \cdot a \sin \left(\frac{\lambda}{2v_{a_n}} (f_{steer} + f_c) \right) - \theta_c \quad (5.7)$$

where

- v_{a_n} = the acoustic velocity of the narrowband steering Bragg cell,
- f_c = the center frequency for the steering Bragg cell, equivalently, the center frequency of the steering signal,
- f_{steer} = the frequency of the steering signal measured from the center frequency of the steering signal,
- θ_c = the nominal angle of deflection out of the steering Bragg cell,

$$\theta_c = 2 \cdot a \sin \left(\frac{\lambda}{2v_{a_n}} f_c \right). \quad (5.8)$$

An expression for the steering frequency as a function of RF array beam angle α is obtained by combining Equations (5.5) and (5.7) to eliminate explicit dependence on the scan angle θ :

$$2a \sin \left(\frac{\lambda}{2v_{a_n}} (f_{steer} + f_c) \right) = a \tan \left[\frac{F_2}{F_1} \frac{1}{F_3} \frac{F_5}{F_4} \frac{b \sin(\alpha)}{c} v_{a_w} \right] + \theta_c,$$

$$f_{steer}(\alpha) = 2 \frac{v_{a_n}}{\lambda} \sin \left[\frac{1}{2} a \tan \left[b \sin(\alpha) \frac{v_{a_w}}{c} \frac{F_5 F_2}{F_4 F_1 F_3} \right] + \frac{\theta_c}{2} \right] - f_c. \quad (5.9)$$

The nominal deflection angle out of the steering Bragg cell is small, and the deflection angle relative to the nominal deflection angle is even smaller. Therefore, a simplified approximation for the steering frequency can be obtained. To obtain this expression, first expand the sine of the sum of two angles in Equation (5.9):

$$f_{steer}(\alpha) = 2 \frac{v_{a_n}}{\lambda} \sin \left[\frac{1}{2} a \tan \left[b \sin(\alpha) \frac{v_{a_w}}{c} \frac{F_5 F_2}{F_4 F_1 F_3} \right] \right] \cos \left(\frac{\theta_c}{2} \right)$$

$$+ 2 \frac{v_{a_n}}{\lambda} \cos \left[\frac{1}{2} a \tan \left[b \sin(\alpha) \frac{v_{a_w}}{c} \frac{F_5 F_2}{F_4 F_1 F_3} \right] \right] \sin \left(\frac{\theta_c}{2} \right) - f_c. \quad (5.10)$$

For $b \sin(\alpha) \frac{v_{a-w}}{c} \frac{F_2 F_1}{F_1 F_1}$ small, Equation (5.10) can be approximated as

$$f_{\text{steer}}(\alpha) \cong \frac{v_{a-n}}{\lambda} b \sin(\alpha) \frac{v_{a-w}}{c} \frac{F_2 F_1}{F_1 F_1} \cos\left(\frac{\theta_c}{2}\right) + 2 \frac{v_{a-n}}{\lambda} \sin\left(\frac{\theta_c}{2}\right) - f_c \quad (5.11)$$

But,

$$2 \frac{v_{a-n}}{\lambda} \sin\left(\frac{\theta_c}{2}\right) = f_c$$

so that Equation (5.11) reduces to

$$f_{\text{steer}}(\alpha) \cong \frac{v_{a-n}}{\lambda} b \sin(\alpha) \frac{v_{a-w}}{c} \frac{F_2 F_1}{F_1 F_1} \cos\left(\frac{\theta_c}{2}\right). \quad (5.12)$$

This expressions shows that the ratios of the focal lengths of the pairs of lenses L1 and L2 can be chosen, based on the relative positions b of the array elements, such that the beams formed by pairs of array elements all propagate in the same direction for a given steering signal frequency.

The required bandwidth of the steering signal, and therefore the steering Bragg cell bandwidth, is

$$B_{\text{steer}} = 2 \cdot f_{\text{steer}}(\alpha_{\text{max}})$$

where the factor of 2 accounts for steering the array up to angle α_{max} to either side of the normal to the RF array. Therefore, in terms of array length, maximum array scan angle from the array normal, lens focal lengths, and steering Bragg cell acoustic velocity, the required steering Bragg cell bandwidth is

$$B_{\text{steer}} \cong 2 \frac{v_{a-n}}{\lambda} b \sin(\alpha_{\text{max}}) \frac{v_{a-w}}{c} \frac{F_2 F_1}{F_1 F_1} \cos\left(\frac{\theta_c}{2}\right). \quad (5.13)$$

The factor

$$\cos\left(\frac{\theta_c}{2}\right)$$

that appears in Equation (5.12) has been left out of Equation (5.13) for bandwidth since it is close to, but less than, unity.

As will now be shown, the expression (5.13) for the bandwidth of the steering Bragg cell can be greatly simplified by imposing the requirement that the width of the steering beam spot on the photodiode be no longer than 1/(signal bandwidth). As will be seen, this simplified expression has no dependence on focal lengths.

The steering beam has a finite width and therefore will spread. The steering beam is assumed to be collimated entering the steering Bragg cell, so the angular spread of the steering beam is determined by the beam profile and the aperture of the steering Bragg cell. If the steering beam were uniform in amplitude across the aperture of the steering Bragg cell, then the angular spread of the steering beam out of the steering Bragg cell would be

$$\frac{2\lambda}{D}$$

where

$$D = \text{aperture of the steering Bragg cell.}$$

Due to this angular spreading, the spot size of the steering beam on the photodiode would be

$$\frac{2\lambda}{D} F_1 \frac{F_3}{F_2}.$$

A uniform weighting results in large sidelobes of the steering beam spot at the photodiodes. The natural profile of the optical beam at the steering Bragg cell is Gaussian. The truncation of the Gaussian by the aperture of the steering Bragg cell is chosen so as to reduce the sidelobes of the steering beam spot at the expense of broadening the spot size on the detector. Therefore the spot size can be expressed as

$$\text{spot size} = \frac{2\lambda}{D} s F_1 \frac{F_3}{F_2} \quad (5.14)$$

where

$$s = \text{ratio of actual spot size at the detector compared to what it would be for uniform weighting across the aperture of the steering Bragg cell.}$$

The steering beam spot size, measured in units of time, must be no larger than $1/(\text{signal bandwidth})$ in order that the time delay processor not bandwidth limit the signal being delayed. That is, from Equation (5.4) the constraint or reference beam spot size is

$$\text{spotsize} \leq \frac{1}{B_{\text{signal}}} v_{a_w} \frac{F_5}{F_4} \quad (5.15)$$

where

B_{signal} = bandwidth of the signal being delayed.

Substitute expression (5.14) for actual spot size into the inequality (5.15) to eliminate the explicit dependence on spot size:

$$\frac{2\lambda}{D} s F_1 \frac{F_3}{F_2} \leq \frac{1}{B_{\text{signal}}} v_{a_w} \frac{F_5}{F_4} \quad (5.16)$$

Rearrange this inequality to collect factors that appear in the expression (5.13) for bandwidth of the steering Bragg cell:

$$\frac{1}{\lambda} v_{a_w} \frac{F_5}{F_4} \frac{F_2}{F_1} \frac{1}{F_3} \geq 2s \frac{B_{\text{signal}}}{D} \quad (5.17)$$

Inequality (5.17) and Equation (5.13) are combined to obtain an expression for the bandwidth of the steering Bragg cell that is independent of the focal lengths of the lenses in the system:

$$B_{\text{steer}} \geq 4s \frac{v_{a_n}}{\lambda} b \sin(\alpha_{\text{max}}) \frac{1}{c} \frac{B_{\text{signal}}}{D} \quad (5.18)$$

This expression for steering Bragg cell bandwidth can be further simplified. Note that the aperture of the steering Bragg cell is given by

$$T_{\text{steer}} = \frac{D}{v_{a_n}} \quad (5.19)$$

and that

$$2 \frac{b \sin(\alpha_{\max})}{c} = T_{\text{signal}}$$

so that the minimum allowed time-bandwidth product of the steering Bragg cell is simply $(2s)$ times the time bandwidth product of the signal Bragg cell:

$$B_{\text{steer}} T_{\text{steer}} = 2s \cdot T_{\text{signal}} B_{\text{signal}} . \quad (5.20)$$

As indicated in Section 4.5.4, a good choice for s is 2 in which case the time-bandwidth product of the steering Bragg cell is simply 4 times the time-bandwidth product of the signal Bragg cell.

Constraints on Focal Lengths of the Lenses

There are pairs of lenses L1 and L2 in the steering leg of the processor to provide angle amplification of the steering beam. The number of pairs of these lenses is equal to the number of time delays to be generated, that is, equal to the number of antenna array elements. The constraints on the focal lengths of the lenses L1 and L2 are that the sum of the focal lengths be the same for each pair, and that the ratio of the focal lengths for each pair be proportional to the ratio of the separations between the corresponding array elements and the reference array element. These constraints can be expressed as:

$$F_{1_i} + F_{2_i} = L \quad (5.21)$$

and

$$d_i \frac{F_{2_i}}{F_{1_i}} = \text{const} \quad (5.22)$$

where

- i = subscript for the i th antenna array element,
- d_i = the separation between the reference and i th antenna array element,
- F_{1_i} = the focal length of the i th L1 lens,

- F_{2i} = the focal length of the i^{th} L2 lens,
 const = a constant independent of i ,
 L = a constant independent of i .

The constraint given by Equation (5.22) is evident from Equation (5.9) for the frequency of the steering signal in terms of the scan angle of the array. From Equation (5.9) it is clear that if constraint (5.22) is met, then each of the pairs of antenna array elements will form a beam in the same direction for a given steering frequency.

A scheme for choosing a value for the constant const is outlined as follows. Let

- 1 = the index for the array element nearest the reference element,
 N = the index for the array element farthest from the reference element.

From Equation (5.22) it is clear that

$$d_1 \frac{F_{2_1}}{F_{1_1}} = d_N \frac{F_{2_N}}{F_{1_N}}. \quad (5.23)$$

With the assumption

$$\frac{F_{2_N}}{F_{1_N}} = \frac{F_{1_1}}{F_{2_1}} \quad (5.24)$$

the ratio of the focal lengths of lens L2 to that of L1 of the lens pair corresponding to the antenna array element nearest the reference element is given by

$$\frac{F_{2_1}}{F_{1_1}} = \sqrt{\frac{d_N}{d_1}}. \quad (5.25)$$

Therefore, given the assumption stated by Equation (5.24), the constant in Equation (5.22) in terms of the minimum and maximum distances between array elements is

$$\text{const} = \sqrt{d_1 d_N}. \quad (5.26)$$

Using Equations (5.21) and (5.22), and Equation (5.26) for const, the expressions for computing the focal lengths for lenses L1 and L2 are

$$F_{2_i} = \frac{L \sqrt{d_1 d_N}}{\sqrt{d_1 d_N + d_i}}, \quad (5.27)$$

$$F_{1_i} = L - F_{2_i}. \quad (5.28)$$

A key advantage of using the convention described above for selecting the focal lengths of lenses L1 and L2 is that it minimizes extremes in the values of the focal lengths. Furthermore, it can be shown that the longest focal length for lens L2 is equal to the longest focal length for lens L1, and the shortest focal length for lens L2 is equal to the shortest focal length for lens L1. That is,

$$F_{2_n} = F_{1_i} \quad (5.29)$$

and

$$F_{2_i} = F_{1_n}. \quad (5.30)$$

The mutual constraints on the focal lengths for lenses L3, L4, and L5, once the focal lengths of lenses L1 and L2 have been selected, are such as to maintain the requirement that the spot size of the steering beam on the photodiode is no wider than $1/(\text{signal bandwidth})$ in terms of the magnified image of the signal Bragg cell on the photodiode. Specifically, from Equation (5.13) together with Equation (5.20), the constraints on the focal length of lens L4 in terms the focal lengths of the other lenses as well as the acoustic velocity of the wideband Bragg cell, the aperture of the steering Bragg cell, the spreading factor of the reference beam, optical wavelength, and signal Bandwidth is the following:

$$F_4 \leq \frac{v_{a_w} D}{2 s \lambda B_{\text{signal}}} \frac{F_{2_1} F_5}{F_{1_1} F_3} \quad (5.31)$$

where

$$\frac{F_{2,1}}{F_{1,1}} \tag{5.32}$$

is the minimum ratio of the focal lengths of lenses L2 and L1. The focal length of lens L4 needs to be kept as small as practical so that, in part, D can be kept small. The larger D the smaller the F-numbers of lenses L1 (and L2).

Using a signal Bragg cell having a large acoustic velocity has two benefits: it helps to keep the F-number of lens L4 from being too small, since the higher the acoustic velocity the smaller the range of diffraction angles out of the signal Bragg cell, and a larger acoustic velocity helps to keep the focal length of lens L4 from becoming too small. Additionally, Equation (5.31) indicates that the ratio of focal lengths of lens L5 to lens L3 should be large.

5.3.2 Example Lens and Bragg Cell Parameter Values

In this section values for the focal lengths and Bragg cell parameters that satisfy the strawman requirements are presented. These example values assume that the value of s, the value of the point spread function for the steering beam spot, is 2 and that the optical wavelength is .84 μm .

Wideband signal Bragg cell parameters:

v_{a_w}	(acoustic velocity)	=	6.31 micron/nanosec (LiNbO ₃)
B_{signal}	(bandwidth)	=	1.0 GHz
T_{signal}	(time aperture)	=	11.5 nanosec
(BT product of signal Bragg cell)		=	11.5)

Steering Bragg cell parameters:

v_{a_n}	(acoustic velocity)	=	.617 mm/micros (slow shear TeO ₂)
B_{steer}	(bandwidth)	=	4.0 MHz
T_{steer}	(time aperture)	=	11.6 microsec
(BT product of steering Bragg cell)		=	45.4)
D	(aperture)	=	7.16 mm

Focal lengths:

F_1	=	72 and 228 mm,
F_2	=	228 and 72 mm,
F_3	=	25 mm,
F_4	=	50 mm,
F_5	=	200 mm.

5.3.3 Phase Adjustment Wedge Parameters

In this section the requirements on the phase adjustment wedge in the steering leg of the time delay architecture shown in Figure 5-1 are developed and specifications are presented.

The wedge angle, the tolerance for this angle, the index of refraction tolerance, and the required surface flatness of the phase adjustment wedge were determine for the following strawman array and demonstration unit design parameters:

Strawman array parameters:

Overall length of array	2 meters
RF of the array	10 GHz
Scan angle range of the array	± 60 degrees

Design parameters:

Index of refraction of phase correction wedge	1.5
Width of photodiode (width of wedge)	500 μm
Phase error budget (same for bias and random)	18 degrees
Bandwidth of the steering signal (approximate)	4 MHz
Intermediate frequency	2 GHz

In addition, this analysis provides a tolerance on the knowledge of the optical wavelength.

The tolerances on the phase correction wedge parameters are based on the effects that uncertainties, both random and biases, have on the power and width of the main beam formed by the RF array. Random phase errors between the array elements reduce the power at the center of the main lobe of the antenna, rather than broadening the main lobe. Biases in phase cause broadening of the main lobe.

Phase Error Budget

An error budget is now established for those contributors to phase errors that are random and for those that are biases.

The result of random phase errors on the signals feeding the array elements of an array with a large number of array elements is to reduce the power in the main beam and to spread this energy across the sidelobes of the array beam pattern. The relative power reduction at the center of the main beam is given by ¹⁷

$$\left\langle \frac{P}{P_0} \right\rangle = e^{-\sigma_p^2} \quad (5.33)$$

where σ_p^2 is the variance of the phase, P is the power on the axis of the main beam when phase errors are present, and P_0 is the power on the main beam axis when there is no variance in the phases. The effect of normally distributed random phase errors with a standard deviation of 18 degrees is to reduce the main beam power at the peak by 10%, compared to no phase errors. The contributor of the phase correction wedge to phase variance is surface nonuniformity of the faces of the wedge. To limit the contribution of the phase correction

wedge to a phase variance of 18 degrees or less requires that the surfaces of the wedge be flat to 1/20 the optical wavelength.

Phase errors that are biases result in a broadening of the beam, since in this case the carrier and envelope of the signal try to form beams in different directions. The desired phase difference between the signal at the reference array element and the signal at the array element a distance d from the reference element is

$$\phi = 2\pi \cdot \frac{d \cdot \sin(\alpha)}{\lambda_{RF}} \quad (5.34)$$

where

d = separation between two elements of the array, one being the reference element,

λ_{RF} = wavelength of the RF signal transmitted (received) by the array,

α = angle of the RF beam measured from the normal to the array.

Deviations in phase, $\delta\phi$, and deviations in phase steered beam angle, $\delta\alpha$, are related by

$$\delta\phi = 2\pi \cdot \frac{d \cdot \cos(\alpha)}{\lambda} \cdot \delta\alpha \quad (5.35)$$

From this expression it is seen that the beam spread relative to the width of the beam, Δ , is equal to the phase bias error measured in units of 2π radians:

$$\frac{\delta\alpha}{\Delta} = \frac{\delta\phi}{2\pi} \quad (5.36)$$

For example, a phase bias of 18 degrees results in a broadening of the main beam by 1/20 the diffraction limited beamwidth Δ .

From the above analysis phase errors of 18 degrees will result in:

Worst case beam broadening of 1/20 diffraction limited beamwidth, phases not necessary random from element to element,

Worst case reduction of 10% in main lobe power for a array with a large number of elements having random phase errors.

Contributors to bias phase errors include errors in the index of refraction of the phase correction wedge, and orientation of the wedge, as well as errors in the optical wavelength. It was determined that the phase changes that result from the change in the IF of the time delayed signals due to the Doppler of the steering signal is insignificant.

Parameter Values and Tolerances

Given the strawman design parameters the following are the parameter values and their tolerances for the phase correction wedge and the optical wavelength that will minimize random and bias phase errors introduced by the phase correction wedge to values no greater than 18 degrees:

Wedge angle	17.243 ± .005 degrees
Flatness of surfaces	1/20 optical wavelength
Angular orientation	± 1.2 degrees
Index of refraction of the wedge	1.50 ± .0002
Optical wavelength	.830 ± .0002 microns

Errors in wedge angle, index of refraction, and optical wavelength can be compensated for to a limited degree by adjusting the orientation of the wedge.

5.4 Optical Efficiency, Detector Characteristics, and SNR

The signal-to-noise ratio (SNR) of the time delay system is a function of the number of signal photons that contribute to the electrical output signal and by the characteristics of the photodetector. In this section an estimate of the SNR of the system based on the system optical efficiency and photodetector characteristics is presented.

The total number of photoelectrons generated in the photodetector is given by

$$m_T = \eta_Q \cdot \left[|O_{\text{signal}}|^2 + |O_{\text{steer}}|^2 + 2 \cdot \text{Real}(O_{\text{signal}} \cdot O_{\text{steer}}^*) \right], \quad (5.37)$$

where integration across the photodetector is assumed. Here

O_{signal} = the complex amplitude of the optical signal from the signal leg that reaches the photodetector,

O_{steer} = the complex amplitude of the optical signal from the steering (reference) leg that reaches the photodetector,

η_Q = the quantum efficiency of the photodetector.

It is only within the steering beam spot on the detector that the heterodyne detection takes place, generating the desired time delayed signal (from the third term in Equation (5.37)). Light falling on the detector outside the reference beam spot contributes to shot noise. Within the steering beam spot the first two terms in Equation (5.37) provide a DC bias that allows negative values of the signal to be represented.

The number of signal photoelectrons generated is

$$m_s = \eta_Q \cdot 2 \cdot \text{Real}(O_{\text{signal}} \cdot O_{\text{steer}}^*) \quad (5.38)$$

where

η_Q = quantum efficiency of the detector.

The magnitudes of the complex amplitudes of the optical signals from the signal and steering legs are determined by the power of the optical source and by the optical efficiencies of the system. The flux of photons (the amplitude squared of the complex amplitudes) of the signal and steering legs of the optical processor are, respectively,

$$\Phi_{\text{signal}} = \Phi_L \eta_{\text{bs}} \eta_{\text{sig}} \quad (5.39)$$

$$\Phi_{\text{steer}} = \Phi_L (1 - \eta_{\text{bs}}) \eta_{\text{str}} \quad (5.40)$$

where

- Φ_L = the flux of photons out of the laser,
- η_{bs} = the splitting ratio of the beam splitter entering the the Mach-Zehnder interferometer in terms of the ratio of the light that enters the signal leg to that that enters the steering leg,
- η_{sig} = the net optical efficiency from the laser through the signal leg of the interferometer to the photodetector, excluding the splitting ratio of the beam splitter entering the interferometer,
- η_{str} = the net optical efficiency from the laser through the steering leg of the interferometer to the photodetector, excluding the beam splitting ratio of the beam splitter entering the interferometer.

The factors that reduce the efficiencies through the two legs are truncation of the beam by the finite apertures of the signal and steering Bragg cells, the diffraction efficiencies of the Bragg cells, the lost of light between the photodiodes in the array, and scattering from the optical surfaces.

The quantum efficiency and fill factor are largely determined by the construction of the photodiode and are dependent on the manufacturer of the photodiode array. The variations in fill factor turn out to be more significant than the variations in quantum efficiency. The other factors are dependent on the design of the optical system. It is important to note that the relative efficiencies of the two paths (the signal and steering paths) are not equal; the steering path is more optically efficient by a factor of 20, mostly because of the spreading of the signal beam across the photosensor.

Technical specifications for p-i-n photodiode arrays from two competing manufacturers were compared to determine total optical efficiency and resulting SNR. The first photodiode array, from Opto-Electronics, Inc. (OE), was found to be 5 times more optically efficient than the second array from United Detector Technologies (UDT) Sensors, Corp. The source power used as a reference was 100mW provided by a Spectra Diode Labs SDL-5412 laser operating at a wavelength of 840nm. The absolute efficiencies depend on the particular beam splitting ratio and Bragg diffraction efficiencies. In one configuration, for example, the total efficiency of the OE detector array was 2.4×10^{-6} compared to 4.7×10^{-7} for the UDT array. These efficiencies yield optical powers of 240 nW and 47 nW, respectively, at the photodetector. However, the actual optical power contributing to the desired signal is potentially less than this amount, because of the differences between the steering and signal path efficiencies.

SNR is the ratio of the number of electrons generated by the desired optical signal to the mean number of electrons generated by noise in the photosensor. The number of signal electrons generated in a photosensor is proportional to the number of photons which impinge on it. The sources of noise electrons in diode-based photosensors are primarily photon shot noise and Johnson noise. Photon shot noise is a result of the stochastic distribution of the generation of photons and their conversion into electrons. The expected mean number of shot noise-generated electrons is equal to the variance of the number of signal electrons. Johnson noise, also referred to as thermal noise, results from the thermal generation of electrons in a load resistor operating at finite temperature. Johnson noise and load resistance are inversely related, such that the higher the resistor value, the lower the Johnson noise. The SNR of a photosensor with out amplification is given by

$$\text{SNR} = \frac{m_s^2}{m_T + \sigma_q^2} \quad (5.41)$$

where m_s is the number of photogenerated signal electrons, m_T is the number of total photogenerated electrons, and σ_q is a resistance-limited circuit noise parameter based on the noise bandwidth, the load resistance, and the absolute temperature. All of these parameters are measured relative to the time resolution (1/bandwidth) of the detector.

In the case of small signal and low output impedance, the Johnson noise will dominate the denominator of the SNR calculation. In the breadboard system, with a load resistance measured in tens of ohms and at a temperature of 300 K, the resistance-limited Johnson noise dominates the denominator of the SNR calculation. In such a case, gain should be used to enhance the number of detected signal electrons. Gain can be provided in two ways: avalanche photodetection or transimpedance amplification. In either case, the gain introduces amplification to both the signal and the shot noise. The amplification process also introduces an excess noise factor to the shot noise. This excess noise factor F is usually a geometric fraction of the gain G , such that $F = G^{0.3}$.

The advantages of an avalanche photodiode (APD) are only realized in resistance-limited circuits, but offer increased SNR in such cases at high speeds. The disadvantages of APDs are the complexity of their bias voltage circuitry, their relative cost, and the inability to find US manufacturers who sell them and are willing to make custom arrays from them. Transimpedance amplification, on the other hand, is not technologically advanced to the point

where it can be useful for this application. The critical parameter in transimpedance amplifiers is the gain-bandwidth product (GBP). Current values of the GBP in commercial devices are limited to $GBP = 10^9$, whereas the beam steering application requires values of $GBP = 10^{12}$.

The measure of SNR in Equation (5.41) is modified by the presence of gain in the photodetection process such that

$$SNR = \frac{m_s^2 G^2}{m_T \cdot F \cdot G^2 + \sigma_q^2} \quad (5.42)$$

The relative values of m_s and m_T are dependent on the ratio of the amount of light through the steering path to the amount of light through the signal path. This ratio is set by the beamsplitting ratio r which is a measure of the optical power split into the signal path relative to the total amount of light entering the first beamsplitter. The relative light power in the steering path is given by $1 - r$. The signal measure (m_s) is determined by the product of the optical amplitudes at the photodetection site and is thus proportional to $r(1 - r)$. The optimal SNR in a thermal noise-limited photodiode occurs when the beamsplitting ratio is equal to 0.5. However, in circuits in which the thermal noise is negligible or in which gain is present, the optimal splitting ratio will demand more light in the less efficient path. Figure 5-4 presents the SNR plotted as a function of beamsplitting ratio r for 2 cases. The lower curve is the SNR in the case of a p-i-n photodiode from Opto-Electronics showing an optimal splitting ratio of $r = 0.5$. The upper curve is for an APD with a gain of $G = 10$ and noise factor $F = 2$. The APD curve illustrates the shift of the optimal splitting ratio to the vicinity of 0.7, meaning 70% of the optical power should be split into the less efficient signal path.

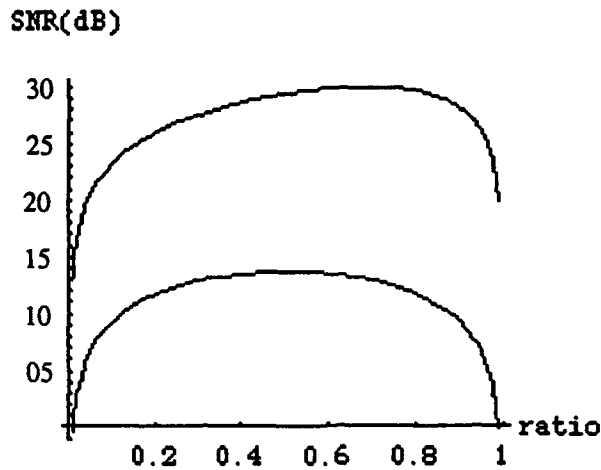


Figure 5-4. System signal-to-noise ratio (SNR) as a function of beamsplitting ratio of light into the steering path relative to the total light. The upper trace is for an APD photosensor array at a gain of 10, and the lower is for a p-i-n photodiode array from Opto-Electronics

The SNR is maximized by the proper selection of the gain G relative to the noise parameter σ_q and the total photo-generated electrons m_T . The optimal choice of the gain is found by equating the Johnson noise to the photon shot noise in the SNR equation and solving for the gain. In the breadboard design, the gain is provided by an avalanche photodiode which has variable gain as set by a bias voltage circuit. An optimal gain of $G = 10$ was found at a beamsplitting ratio of 0.7. The SNR varies very slowly in the vicinity of the optimal gain, allowing SNR performance to within 1% of maximum at gains between $G = 8$ and $G = 12$. The expected SNR versus gain of the APD is shown in Figure 5-5, and peaks at better than 30.0 dB.

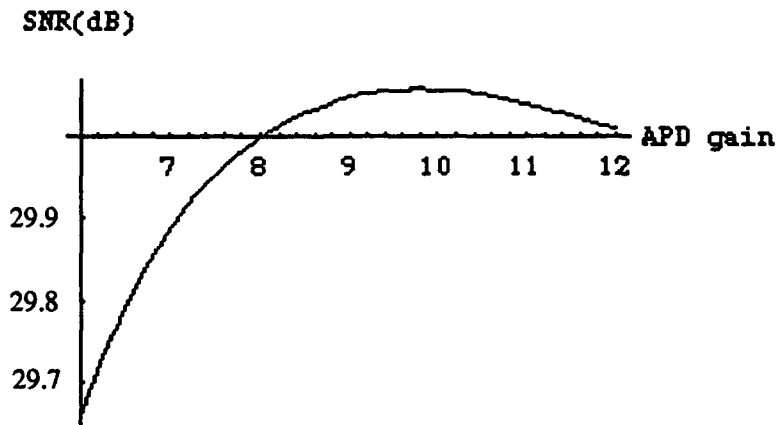


Figure 5-5. Signal-to-noise ratio (SNR) as a function of gain in an APD at a 0.7 beamsplitting ratio

5.5 Scan Angle Sensitivity

Computations to determine the sensitivity of the antenna beam scan angle to changes in the frequency of the steering control signal, and to determine the ability to maintain a narrow beam were performed based on the analytical relations in Section 5.3. Two cases were considered: 1) no angle amplification, 2) angle amplification implemented with lens pairs. The first case is applicable to the use of single-element modules or to the use of a multi-channel steering Bragg cell to create and control the steering signal. The analysis for the second case verifies that the focal lengths of the lenses of the angle amplification lens pairs can be selected such that the RF plane waves generated from pairs of array elements all propagate in the same direction. That is, the angle amplification optics does not result in beam broadening at large beam scan angles.

The example parameter values used in this analysis are the following:

- Four antenna array elements positioned at 0, .2, .4 and 2. meters,
- Signal bandwidth of 1 GHz,
- Photodiode width of 2.9 millimeters,
- Slow shear mode TeO_2 for the beam steering Bragg cell.

5.5.1 No Angle Amplification

Figure 5-6 shows a plot of the antenna beam scan angle, formed by the two end elements of the array (separated by 2 meters), versus the frequency of the steering signal for the case that no angle amplification is used. The values of the control frequency indicated in Figure 5-6 are relative to band center of the steering Bragg cell, here assumed to be 50 MHz. From this plot it is seen that changing the frequency of the steering signal by 4 MHz scans the beam 45 degrees away from the array normal. Controlling the pointing direction of the beam to .1 degrees requires that the frequency of the steering beam be controlled to within approximately 9 kHz for an array element separation of 2 meters. For two elements spaced .2 meters apart, the frequency of the steering signal must be controlled to within approximately 900 Hz in order to maintain the pointing direction of the array to within .1 degrees. These precisions to which the steering frequencies must be controlled are easy to maintain.

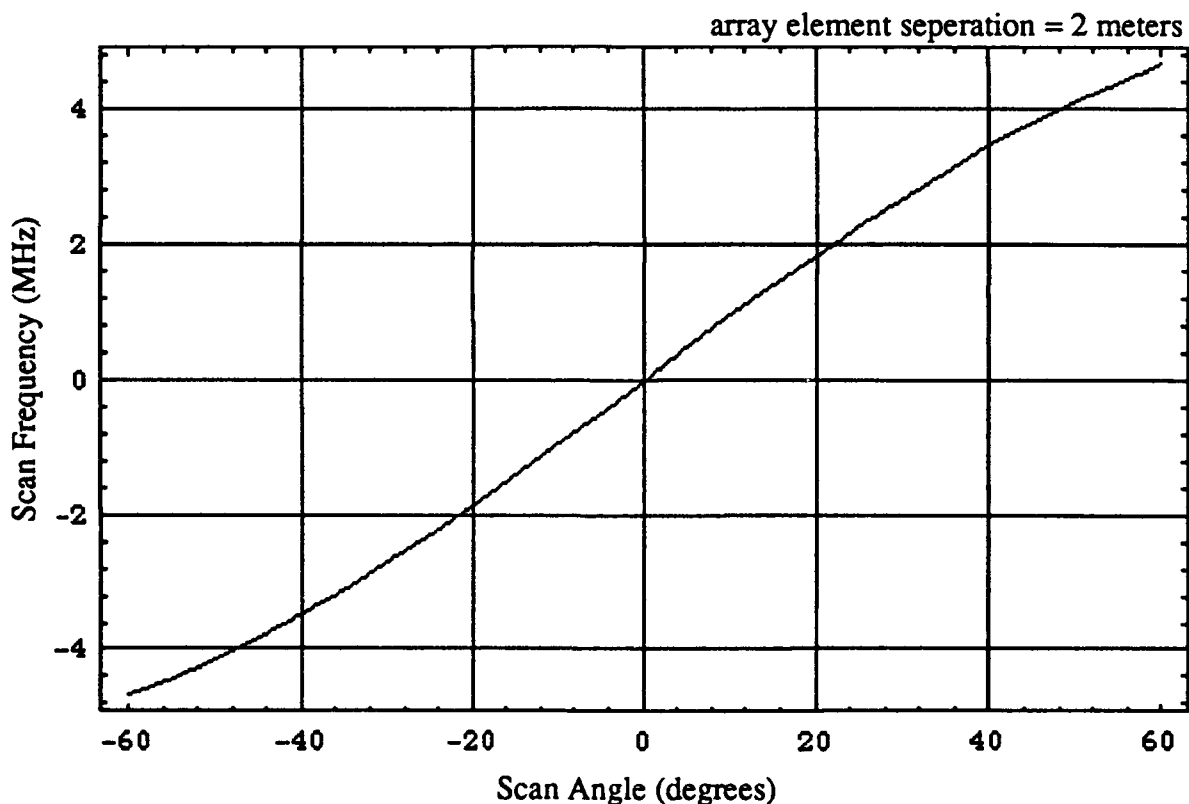


Figure 5-6. Beam Scan Angle versus Steering Control Frequency for no Angle Amplification

5.5.2 Angle Amplification with Lenses

Figure 5-7 shows a plot of the antenna beam scan angle, formed with pairs of elements of the array, versus the frequency of the steering control signal when a single steering Bragg cell and pairs of lenses for angle amplification are used to form and steer the beam of the RF array. The antenna element pair spacings considered are .2, .4, and 2 meters. From this plot it can be determined that controlling the pointing direction of the beam to within .1 degrees requires that the frequency of the steering beam be controlled to within approximately 4 kHz.

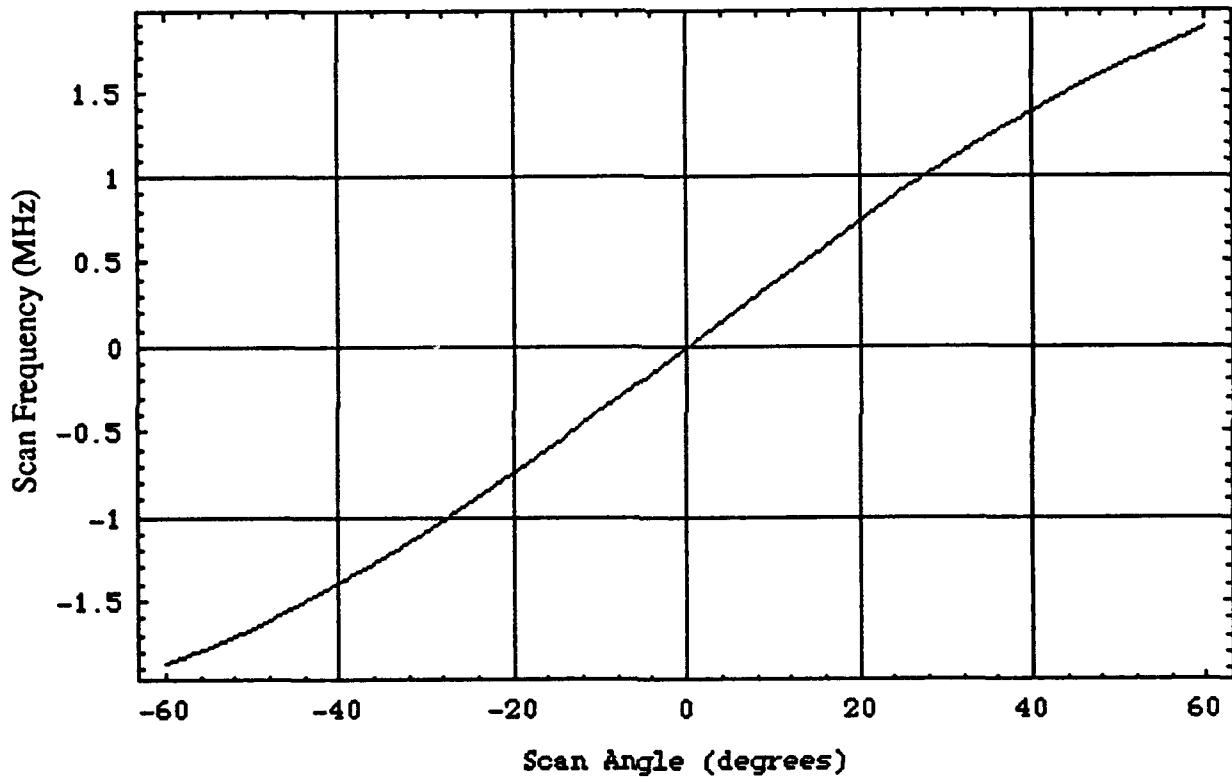


Figure 5-7. Beam Scan Angle versus Steering Control Frequency with Lens Pairs Providing Angle Amplification

Section 6

SUMMARY OF ANALYSIS

In this section the key performance issues of the acousto-optic true time delay beamformer are briefly summarized.

6.1 Beamwidth

The determining factors for the beamwidth of the RF array are the following:

- Size of RF array (length, width),

- Weighting of array elements,

- Closeness of time and phase delays to their ideal values (the factors affected by the true time delay processor).

Analysis shows that the time delays can be controlled to a high degree of precision so that the increase in beamwidth due to inaccuracies in the time delays from the true time delay beamformer should be insignificant.

The phase shift adjustments implemented in the processor to properly translate from the IF of the processor to the RF has the potential to broaden the beam. The breadboard demonstration unit is designed so that the errors in the phase adjustments is to be no greater than 18 degrees. A phase bias error of 18 degrees between end array elements would lead to a beam broadening of 1/20 the diffraction limited beamwidth of the array. Random phase errors having a standard deviation of 18 degrees would lead to a decrease of main beam power by a factor of 1/10.

6.2 FM Spreading

FM spreading is the broadening of the RF beam for a wideband signal when the beam is steered off boresite. FM spreading is a result of:

- Not using true time delay beam steering, or time delays not being correct.

- The phases of the carrier at the RF of the array not having the correct values corresponding to beam direction and RF frequency.

The acousto-optic true time delay beamformer controls correctly and precisely both the time delays and phase shifts of the signal to be transmitted over the full bandwidth of the signal and over wide scan angles. As a result, so FM spreading is eliminated.

6.3 Sidelobes

Spurious low amplitude time delays lead to RF array sidelobes. The contributions of the time delay processor to these sidelobes can be controlled to a desired level with a proper design and implementation.

The strawman design will result in -35 dB sidelobe contributions from spurious time delays. These sidelobe levels are a result of truncating the optical steering beam, which has a Gaussian profile upon entering the steering Bragg cell, such that the largest steering beam spot size on a photodiode is twice as wide as if the truncating aperture were uniformly filled. Lower sidelobe levels can be achieved, if desired, by modifying the optical design to narrow the steering reference beam upon entrance into the steering Bragg cell so that a higher fraction of the width of the Gaussian beam passes through the aperture of the Bragg cell. This requires the design for the optics between the two Bragg cells and the photodiode array be more stringent still maintaining the requirement that the steering beam spot on the photodiode be no wider, in units of delay time, than the reciprocal of the bandwidth of the signal to be delayed.

6.4 Number of Simultaneous Beams

Multiple simultaneous beams are produced by driving the steering Bragg cell with a multi-toned signal, one tone for each beam. The multi-toned signals result in two-tone third-order intermodulation products from the steering Bragg cell, causing unwanted spurious time delays. These intermodulation products can be held to desired low levels by limiting the power of the signal driving the steering Bragg cell. This, however, limits the diffraction efficiency of steering Bragg cell. The system needs to be built with sufficient optical power to compensate for this loss of efficiency if multiple simultaneous beam are to be transmitted.

Contributors to noise on the time delayed signal include:

Photon shot noise,

Johnson noise.

The higher the power in the signal optical beam and the reference optical beam, the higher the signal-to-noise ratio of the time delayed signal. The optical power in the reference beam is effectively divided into the multiple beams. Therefore, for a fixed power optical source, the SNR of the time delayed signals will decrease as the number of simultaneous beams is increased.

The system must be built with sufficient optical power to meet or exceed a set SNR threshold when the number of simultaneous beams is at or less than a set limit.

6.5 Scaling to Large Arrays

Scaling up to arrays with long baselines does not appear to be an issue. Acousto-optics can easily generate long time delays. For example, a 1 GHz signal can be time delayed up to 1 microsecond. An array would have to have a base line of at least 1000 feet to require such long time delays.

The processor can be scaled up to steer arrays with a large number of array elements. For the transmitting-only architectures the number of simultaneous time delays that can be generated per unit is limited by the number of sets of angle amplification optics that can be fabricated and by the number of elements in photodiode array. For the transmitting/receiving architecture, the number of simultaneous time delays per unit is limited by the number of channels in multichannel wideband signal Bragg cell (on the order of 64).

For arrays with more elements than the number of time delays that can be easily generated, the array can be divided into subarrays. Each subarray is then driven with a single time delayed signal. Phase shifts are applied between the elements within each subarray.

6.6 Beam Scanning Rate

The time required to change the beam look direction is the time aperture of the steering Bragg cell. This time is independent of the magnitude of the change of look direction. The longer the time and physical aperture of the steering Bragg cell the easier the optical design, but the longer it takes to change the pointing direction of the array. A longer Bragg cell aperture makes the optical design easier to obtain a small reference beam spot size for the Image Plane architecture, or a flat reference beam phase front for the Fourier Plane architecture. It turns out

that the wider the bandwidth of the signal to be delayed, the longer the desired aperture of the steering Bragg cell.

The time aperture of the steering Bragg cell (the time to change array steering direction) for the strawman design is approximately 10 microseconds. This design is for transmitting a 1 GHz bandwidth signal.

6.7 Beam Scan Accuracy, Range

Beam scan accuracy is determined, for a given set of design parameters, by the accuracy of the steering signal. For a given set of design parameters, beam scan range determines the required bandwidth of the steering Bragg cell. The required bandwidth of the steering signal is quite modest (4 MHz). A .1 degree pointing accuracy requires controlling the steering frequency to within 3.33 kHz, a very modest requirement for the following strawman design parameters:

Array type:	linear,
Signal bandwidth:	1 GHz,
Array scan:	$\pm 60^\circ$ from array normal,
Overall length of array:	2 meters.

6.8 Signal Fidelity

A properly designed optical system implemented with high quality components will be able to maintain signal fidelity. Key design and implementation considerations for the Fourier Plane architecture are the following:

Generate a good quality Fourier transform of the signal Bragg cell on the photodiode array,

Ensure phase flatness of the reference beam on the detector in order not to band limit the signal.

Key design and implementation considerations for the Image Plane architecture are the following:

Generate a good quality image (amplitude and phase) of signal Bragg cell onto the photodiode array,

Ensure small spot size of reference beam on the photodiodes in order to avoid band-limiting the signal.

6.9 Signal-to-Noise

The signal-to-Noise ratio of signals time delayed by the processor is limited by available photonic energy in the optical system. The optical system should be designed to have maximum possible optical efficiency, and use a stabilized laser with highest available power. The demonstration breadboard for demonstrating the feasibility of delaying 1 GHz bandwidth signals is designed to achieve an SNR of 30 dB using a 100 milliwatt optical source and an avalanche photodiode. Follow-on units will be designed to be more light efficient and therefore have higher SNRs.

6.10 RF Bandwidth

The bandwidths of transmit/receive signals are limited to on the order of 2 GHz, the limit of acousto-optics. Bandwidths on the order of 1 GHz and above necessitate more caution in the optical design. As the bandwidth gets wider, focal lengths and F-numbers get small, and photodiodes become noisier.

6.11 Translation from IF to RF

The time delays are generated at the IF of the time delay processor. Additional phase shifts must be imparted to the time delayed signals that are proportional to time delay and the difference between the IF of the processor and the RF of the array. These phase corrections can be implemented within the optical processor with a transparent wedge, as described in Sections 4.2 and 5.3.3.

6.12 RF/Beam Direction Dependence (Independence)

The time delays generated are independent of the RF of the array. However, the phase correction in the processor is dependent on the difference between the IF of the processor and the RF of the array. Thus, if phase corrections are done outside the processor then the RF of the array can be changed. However, if the phase correction is performed in the time delay processor then the RF of the array cannot be changed without changing the phase correction wedge in the processor.

Section 7

RECOMMENDATIONS

Recommendations are made on the structure of the time delay processor. The primary choices are between the Image Plane (time-domain) and Fourier Plane (frequency domain) architectures, and between the single- and multiple-element structures.

The Image Plane architecture offers greater design flexibility and is more consistent with the dependence of photodiode size on bandwidth. Furthermore, for the Image Plane architecture, the required size of the detector tends to decrease with increasing bandwidth which is consistent with the dependence of photodiode size on bandwidth. For the Fourier Plane architecture, on the other hand, the width of the photodiodes needs to increase with increasing signal bandwidth in order to catch the full spectrum of the signal. This is in conflict with the fact that the area of photodiodes decreases as the bandwidth is increased.

The Image Plane architecture requires more optical elements than the Fourier Plane architecture, leading to a larger physical size. However, the additional lenses provide added degrees of freedom in choosing focal lengths and F-numbers which eases the design constraints. This easing of design constraints is particularly valuable for the development of the demonstration breadboard for which the budget is not available for custom designed optical components. Furthermore, size is not an issue for the proof-of-principle demonstration.

The Image Plane architecture is recommended over the Fourier Plane architecture, especially for the case of the proof-of-principle demonstration. In cases where the size of the processor is a primary consideration and a more costly implementation can be afforded, then the Fourier Plane architecture should be reconsidered.

The single-element time delay modules are much simpler and therefore easier and less expensive to manufacture than are the multi-element modules. However, a serious concern with the use of single-element modules is the difficulty of maintaining the relative phase between the time delays, one from each module, to a high degree of accuracy. By contrast the multi-element module naturally controls the relative phases between the time delayed signals to a high degree of accuracy. If only the envelope of the time delayed signals are used, and phase

shifts are provided at the array elements then the draw back of the the single element units to maintain relative phase is irrelevant.

An attractive aspect of the multi-element module is the fact that a single signal (a tone) controls the generation of the time delays, whereas use of single-element modules for beamforming requires the generation of a different control signal for each of the single-element modules.

A requirements analysis and detailed design based on a particular application would need to be performed to determine applicability and relative cost/complexity of the single- and multi-element module approaches.

7.1 Recommended Breadboard Demonstration

The recommended breadboard demonstration system is an Image Plane architecture using a multi-element module for a transmitting array. It will demonstrate that the necessary relationships between the time delays and phases can be maintained to sufficient accuracy to guarantee a narrow beamwidth in the steered beam of the RF antenna array.

Multi-element module proof-of-principle results apply equally well to the single-element module configuration, and, for the most part, to the Fourier plane architecture.

7.2 Final Recommendations

Final architecture configuration recommendations will be made after completion of the demonstration and evaluation of results. These recommendation will be based upon Task 1 analysis, Task 2 results, and identification of a specific set of applications.

Section 8

REFERENCES

1. I. C. Chang and S. S. Tarn, "Phased array beamforming using acousto-optic techniques", *Proceeding SPIE*, vol. 936, pp. 163-167, 1988.
2. D. Dolfi, F. Michel-Gabriel, S. Bann, and J. P. Huignard, "Two-dimensional optical architecture for time-delay beam forming in a phased-array antenna," *Optics Letters*, vol. 16, pp. 255-257, February 1991.
3. G. A. Koepf, "Optical processor for phased-array antenna beam formation," *Proceeding SPIE*, vol. 477, pp. 75-81, 1984.
4. K. A. Nickerson, P. E. Jessop, and S. Haykin, "Optical processor for array antenna beam shaping and steering," *Optical Engineering*, vol. 30, pp. 1497-1502, October 1991.
5. N. A. Riza and D. Psaltis, "Acousto-optic signal processors for transmission and reception of phased-array antenna signals," *Applied Optics*, vol. 30, pp. 3294-3303, August 1991.
6. N. A. Riza, "A transmit/receive time delay optical beamforming architecture for phased array antennas," *Applied Optics*, vol. 30, pp. 4594-4595, November 1991.
7. _____, "An acoustooptic phased array antenna beamformer with independent phase and carrier control using single sideband signals," *IEEE Photonics Technology Letters*, vol. 4, pp. 177-179, February 1992.
8. _____, "Acousto-optic architecture for two-dimensional beam scanning in phased-array antennas," *Applied Optics*, vol. 31, pp. 3278-3284, June 1992.
9. _____, "An acoustooptic-Phased-array antenna beamformer for multiple simultaneous beam generation," *IEEE Photonics Technology Letters*, vol. 4, pp. 807-809, July 1992.
10. E. N. Toughlin, H. Zmuda, and P. Kornreich, "A deformable mirror-based optical beamforming system for phased array antennas," *IEEE Photonics Technology Letters*, vol. 2, pp. 444-446, June 1990.
11. R. T. Weverka, K. Wagner, and A. Sarto, "Optical processing for self-cohering of phased-array imaging radars," *Proceeding SPIE*, vol. 1703, pp 552, 1992.
12. L. H. Gesell and J. L. Lafuse, "True time delay beam formation," patent application, serial no. 07/806,697, December, 1991.
13. L. H. Gesell and T. M. Turpin, "True time delay beam forming using acousto-optics," *Proceeding SPIE*, vol. 1703, 1992.
14. A. Vander Lugt, "Interferometric spectrum analyzer," *Applied Optics*, vol. 20, pp. 2270-2279, August 1981.

15. P. J. Roth, "Optical excision in the frequency plane," *Proceeding SPIE*, vol. 352, pp. 17-23, 1982.
16. J. L. Lafuse, "Optical correlation using the Excisor detector," *Proceeding SPIE*, vol. 352, pp. 24-27, 1982.
17. B. D. Steinberg, Microwave Imaging with Large Antenna Arrays, pp. 32-37, John Wiley and Sons, 1983.

***MISSION
OF
ROME LABORATORY***

Mission. The mission of Rome Laboratory is to advance the science and technologies of command, control, communications and intelligence and to transition them into systems to meet customer needs. To achieve this, Rome Lab:

- a. Conducts vigorous research, development and test programs in all applicable technologies;
- b. Transitions technology to current and future systems to improve operational capability, readiness, and supportability;
- c. Provides a full range of technical support to Air Force Materiel Command product centers and other Air Force organizations;
- d. Promotes transfer of technology to the private sector;
- e. Maintains leading edge technological expertise in the areas of surveillance, communications, command and control, intelligence, reliability science, electro-magnetic technology, photonics, signal processing, and computational science.

The thrust areas of technical competence include: Surveillance, Communications, Command and Control, Intelligence, Signal Processing, Computer Science and Technology, Electromagnetic Technology, Photonics and Reliability Sciences.